

Transcriptional landscape of cotton roots in response to salt stress at single-cell resolution

Pengtao Li^{1,2,3,8}, Qiankun Liu^{1,2,4,8}, Yangyang Wei^{1,8}, Chaozhu Xing^{2,3,8}, Zhongping Xu⁵, Fang Ding⁶, Yuling Liu¹, Quanwei Lu¹, Nan Hu¹, Tao Wang¹, Xiangqian Zhu⁵, Shuang Cheng^{1,4}, Zhaoguo Li^{1,4}, Zilin Zhao¹, Yanfang Li¹, Jiangping Han², Xiaoyan Cai², Zhongli Zhou², Kunbo Wang², Baohong Zhang⁷, Fang Liu^{2,3,*}, Shuangxia Jin^{5,*} and Renhai Peng^{1,3,4,*}

¹College of Biology and Food Engineering, Anyang Institute of Technology, Anyang, Henan 455000, China

²State Key Laboratory of Cotton Biology, Institute of Cotton Research, Chinese Academy of Agricultural Sciences, Anyang, Henan 455000, China

³Research Base, Anyang Institute of Technology, State Key Laboratory of Cotton Biology, Anyang 455000, Henan, China

⁴School of Life Sciences, Zhengzhou University, Zhengzhou, Henan 450001, China

⁵Hubei Hongshan Laboratory, National Key Laboratory of Crop Genetic Improvement, Huazhong Agricultural University, Wuhan, Hubei, China

⁶Hubei Key Laboratory of Plant Pathology, Huazhong Agricultural University, Wuhan, Hubei 430070, China

⁷Department of Biology, East Carolina University, Greenville, NC 27858, USA

⁸These authors contributed equally to this article.

*Correspondence: Fang Liu (liufcri@163.com), Shuangxia Jin (jsx@mail.hzau.edu.cn), Renhai Peng (aydxprh@163.com)

<https://doi.org/10.1016/j.xplc.2023.100740>

ABSTRACT

Increasing soil salinization has led to severe reductions in plant yield and quality, and investigating the molecular mechanism of salt stress response is therefore an urgent priority. In this study, we systematically analyzed the response of cotton roots to salt stress using single-cell transcriptomics technology; 56 281 high-quality cells were obtained from 5-day-old lateral root tips of *Gossypium arboreum* under natural growth conditions and different salt treatments. Ten cell types with an array of novel marker genes were identified and confirmed by *in situ* RNA hybridization, and pseudotime analysis of some specific cell types revealed their potential differentiation trajectories. Prominent changes in cell numbers under salt stress were observed for outer epidermal and inner endodermal cells, which were significantly enriched in response to stress, amide biosynthetic process, glutathione metabolism, and glycolysis/gluconeogenesis. Analysis of differentially expressed genes identified in multiple comparisons revealed other functional aggregations concentrated on plant-type primary cell wall biogenesis, defense response, phenylpropanoid biosynthesis, and metabolic pathways. Some candidate differentially expressed genes encoding transcription factors or associated with plant hormones also responsive to salt stress were identified, and the function of *Ga03G2153*, annotated as auxin-responsive *GH3.6*, was confirmed by virus-induced gene silencing. The *GaGH3.6*-silenced plants showed a severe stress-susceptible phenotype, and physiological and biochemical measurements indicated that they suffered more significant oxidative damage. These results suggest that *GaGH3.6* might participate in cotton salt tolerance by regulating redox processes. We thus construct a transcriptional atlas of salt-stressed cotton roots at single-cell resolution, enabling us to explore cellular heterogeneity and differentiation trajectories and providing valuable insights into the molecular mechanisms that underlie plant stress tolerance.

Key words: cotton, salt stress, scRNA-seq, root cell types, virus-induced gene silencing

Li P., Liu Q., Wei Y., Xing C., Xu Z., Ding F., Liu Y., Lu Q., Hu N., Wang T., Zhu X., Cheng S., Li Z., Zhao Z., Li Y., Han J., Cai X., Zhou Z., Wang K., Zhang B., Liu F., Jin S., and Peng R. (2024). Transcriptional landscape of cotton roots in response to salt stress at single-cell resolution. *Plant Comm.* **5**, 100740.

INTRODUCTION

Plants are constantly subjected to various biotic and abiotic stresses throughout their life cycle (Atkinson and Urwin, 2012). Owing to the complexity and variability of field environments, as well as interactions with other factors, multiple stresses strongly impact the germination, growth, and reproduction of sessile organisms. This triggers various morphological, physiological, and biochemical changes, leading to incalculable yield losses and quality reduction (Bray et al., 2000). Plants have developed a complex and precise regulatory system for surviving and adapting to adversity, which normally begins with signal perception, followed by the production of signaling molecules and stimulus responses at the plasma membrane of plant cells (Zhang et al., 2020). Subsequently, reactive oxygen species (ROS), phosphatidylinositol, and/or other secondary signaling molecules stimulate the intracellular membranes, initiate a protein phosphorylation cascade by regulating Ca^{2+} levels, and produce phosphorylated protein molecules that target important proteins directly involved in cell protection or crucial transcription factors (TFs) relevant to specific stress-regulated genes (Gong et al., 2020). Some genes participate in the biological synthesis of regulatory factors such as abscisic acid (ABA) and ethylene, thus activating the expression of TFs that bind specifically to the promoter sequences of target genes to further activate or inhibit the expression of downstream functional genes, ultimately playing major roles in response to abiotic stress (Zhang et al., 2022a, 2022b, 2022c). Revealing the regulatory mechanisms of plant responses to environmental conditions and cultivating novel varieties of stress-resistant crops will not only promote the sustainable development of modern agriculture but also ensure food security in the face of a rapidly expanding world population (Zhu, 2016).

Soil salinization is one of the global challenges that limit land usage and crop production, impacting approximately 20% of irrigated land globally (Morton et al., 2019). Salt stress significantly inhibits seed germination, root length, plant height, and fructification (Liang et al., 2014). Signals are first perceived by the cell wall, after which cell wall damage and compositional changes trigger the production of secondary messengers such as Ca^{2+} and ROS in response to salt stress. Differential gradients of Na^+ and K^+ between the cytoplasm and the extracellular space then affect salt overly sensitive genes via Ca^{2+} to prevent cell damage and nutrient loss, and ROS signaling sensors activate MAPK cascades, ROS-scavenging pathways, and some salt-resistance genes to remove excess superoxide anions. Finally, ion equilibrium and ROS homeostasis can help plants to generate salt tolerance (Liang et al., 2018). Some phytohormones and TFs have been reported to participate in coordinating various signal transduction pathways of salt-stress responses, including those related to ABA, cytokinins, ethylene, salicylic acid, and jasmonic acid (JA) (Yu et al., 2020), as well as AP2/EREBP, WRKY, NAC, MYB, GRAS, and ZIP TFs (Hoang et al., 2017). All this progress has helped to elucidate the molecular mechanisms by which plants respond to salt stress at a single-cell resolution.

Single-cell RNA sequencing (scRNA-seq) technology has not only overcome the limitations of bulk RNA-seq in characterizing cell uniqueness or heterogeneity but also enabled the discovery of previously unknown abilities and undescribed states of cells

Transcriptional landscape of cotton roots

(Tang et al., 2009). This has helped us to investigate the molecular mechanism of network regulation between intercellular genes and the transcriptome trajectory of cell fate selection and organogenesis (Wen and Tang, 2022). In general, scRNA-seq technology can be divided into three broad categories: plate based, droplet based, and combinatorial indexing (Birnbaum 2018). A droplet-based strategy such as 10x Genomics uses microfluidic technology to capture single cells and has the advantages of easier operation, higher throughput, and lower cost compared with other technologies (Zheng et al., 2017). It is therefore the most widely used strategy in the reported literature (Seyfferth et al., 2021). Since the first report of scRNA-seq in *Arabidopsis thaliana* (Shulse et al., 2019), there have been dozens of published articles relevant to single-cell sequencing in plants, including *A. thaliana* (Zhang et al., 2019a, 2019b, 2021a, 2021b, 2019b; Denyer et al., 2019; Jean-Baptiste et al., 2019; Ryu et al., 2019; Turco et al., 2019; Liu et al., 2020, 2022a, 2022b, 2022c, 2022d; Wendrich et al., 2020, 2021b; Gala et al., 2021, 2022b; 2022c, 2022d; Shaham et al., 2022), rice (Liu et al., 2021a, 2021b, 2021c; Wang et al., 2021a, 2021b, 2021c), maize (Nelms and Walbot, 2019; Satterlee et al., 2020; Xu et al., 2021), poplar (Li et al., 2021a, 2021b; Xie et al., 2022), peanut (Liu et al., 2021a, 2021b, 2021c), tomato (Tian et al., 2020; Omary et al., 2022), cotton (Qin et al., 2022; Long et al., 2023; Sun et al., 2023), and strawberry (Bai et al., 2022), and involving the root, stem, leaf, flower, cotton fiber and gland, stem tip, ear, and cotyledon tissues/organs. However, scRNA-seq analyses of plant stress responses are still very limited (Jean-Baptiste et al., 2019; Liu et al., 2022a; 2022b, 2022c, 2022d; Cao et al., 2023). Overall, five major achievements have been obtained from these scRNA-seq analyses: (1) obtaining single-cell resolution by identifying cell types and verifying marker genes (Liu et al., 2021a, 2021b, 2021c; Zhang et al., 2021a, 2021b), (2) deducing developmental trajectories by comparing expression levels of different genes in single cells and ordering the positions of different cell types during development (Shulse et al., 2019; Li et al., 2021a, 2021b), (3) investigating the regulatory mechanisms of plant responses to various stresses by identifying changes in cell types and expression patterns of key functional genes between samples from natural and stressed conditions (Wendrich et al., 2020; Liu et al., 2022a, 2022b, 2022c, 2022d), (4) exploring the conservation and diversity of developmental programs among different species by comparing single-cell profiles between different subspecies of the same species or between the same tissues of different species (Liu et al., 2020; Zhang et al., 2021a, 2021b), and (5) performing combined analyses with multiple omics technologies to explain specific biological processes by combining RNA-seq and ATAC-seq at the single-cell level (Farmer et al., 2021; Marand et al., 2021). Notably, our group developed an integrated online tool to explore the single-cell plant transcriptome landscape, called the Plant Single Cell Transcriptome Hub (PsctH), which includes a method for protoplast isolation, a pipeline for data processing, and a manually curated resource of cell markers collected from experimental research (Xu et al., 2022).

To characterize the transcriptional landscape of plants under natural and salt-stressed conditions at a single-cell resolution, we used an optimized method of protoplast dissociation to obtain

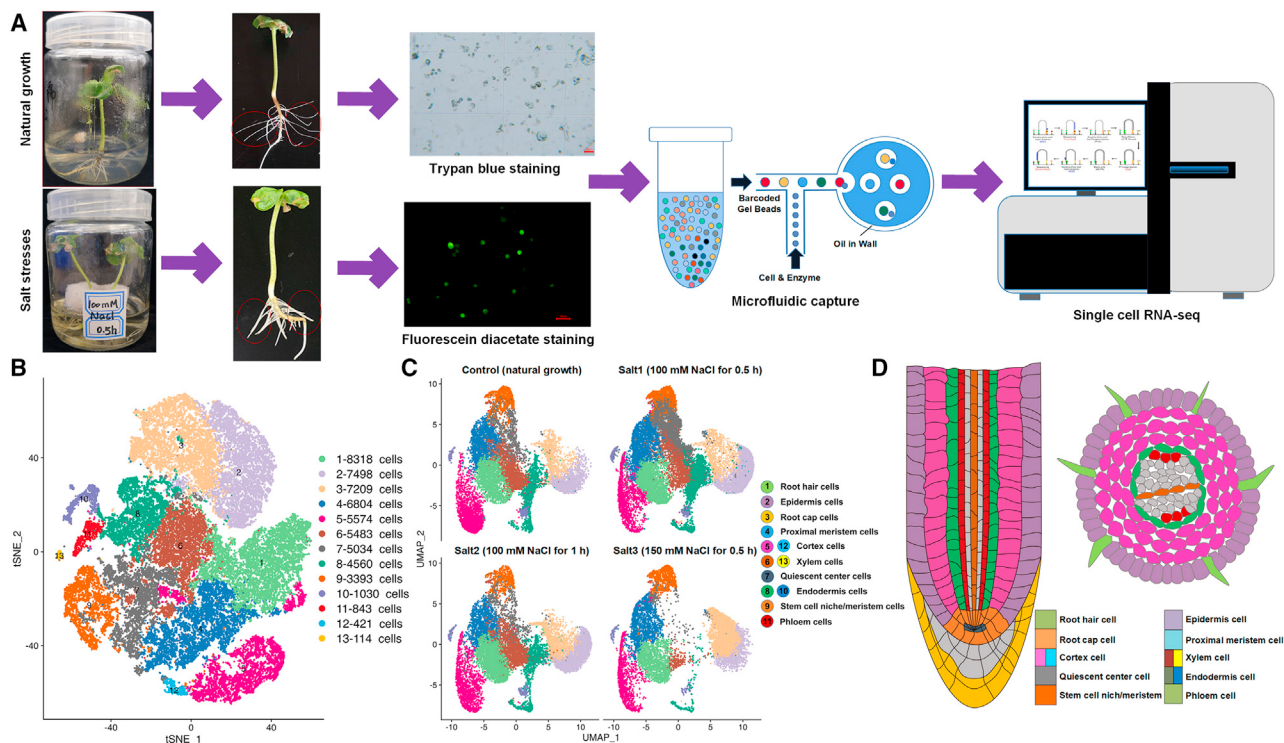


Figure 1. Single-cell RNA-seq and cluster annotation of cotton lateral root tips.

(A) Overview of cotton scRNA-seq and Illumina sequencing workflow.

(B) t-SNE visualization of putative clusters from cotton lateral root tips.

(C) UMAP visualization of predicted cell types from cotton lateral root tips under natural growth conditions (control), 100 mM NaCl for 0.5 h (salt1), 100 mM NaCl for 1 h (salt2), and 150 mM NaCl for 0.5 h (salt3).

(D) Longitudinal and transverse diagrams of different cell types in cotton lateral root tips.

cells from the lateral root tips of *G. arboreum*. This diploid ancestor (A_2) of cultivated cotton is not only an economically important crop for natural fiber and edible oil production worldwide but also a significant pioneer plant for salt and alkali tolerance (Wendel et al., 2012; Zhao et al., 2020). We compared samples exposed to the same salinity concentration for different durations or different salinity concentrations for the same duration to identify diverse cell clusters and corresponding marker genes, and pseudotime analysis was used to characterize development and differentiation. Through the combined identification of functional genes, signal pathways, plant hormones, and TFs related to salt stress, this work provides a solid foundation for further resolving the molecular mechanisms of plant salt-stress responses.

RESULTS

Construction of a single-cell transcriptional atlas of cotton roots under salt stress

Using our optimized dissociation method (Liu et al., 2022a, 2022b, 2022c, 2022d), high-quality protoplasts were isolated and confirmed by trypan blue and fluorescein diacetate staining (supplemental Figure 1); total RNA was then extracted from the high-quality protoplasts and used for scRNA-seq on the 10x Genomics platform (Figure 1A). Four treatments were performed: control (natural growth), salt1 (100 mM NaCl stress for 0.5 h), salt2 (100 mM NaCl stress for 1 h), and salt3 (150 mM NaCl stress for 0.5 h). A total of 61 095 single cells and an average of

7637 cells per sample were obtained according to primary QC (quality control) of the sequenced data with Cell Ranger (supplemental Table 1). Double or multiple cells (also called doublets) and unbound or apoptotic cells were removed, as were cells with high mitochondrial gene expression and those strongly influenced by the cell life cycle (supplemental Excel 1) or enzymatic hydrolysis (supplemental Excel 2). A total of 56 281 high-quality cells and an average of 7035 cells per sample were thus retained for further bioinformatic analyses (supplemental Figure 2). Pearson correlation coefficient (PCC) analyses were performed on both bulk and single-cell RNA-seq data (supplemental Figure 3A–3C). In most cases, the three biological replicates of undissociated tissues or dissociated protoplasts from bulk RNA-seq had correlation coefficients of approximately 98%, and the two biological replicates of dissociated protoplasts from scRNA-seq had correlation coefficients of approximately 80%. Transcriptome samples from the same treatment were also subjected to PCC analysis (supplemental Figure 3D), and the correlation coefficients between the dissociated protoplasts from the bulk and scRNA-seq samples were higher than those between the undissociated tissues from the bulk RNA-seq samples and dissociated protoplasts from the scRNA-seq samples. Taken together, these data confirmed the high quality and reliability of the scRNA-seq data.

Dimensionality reduction was first applied on approximately 2000 genes (average nGene) using the mutual nearest neighbors algorithm. Cell clustering was performed and visualized using t-SNE

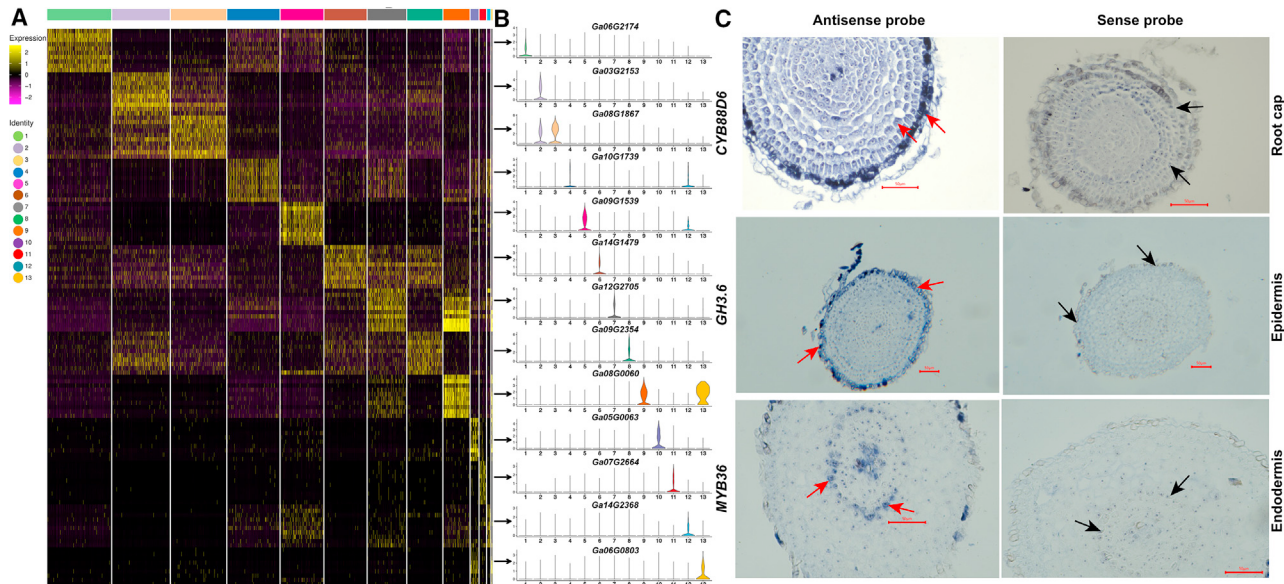


Figure 2. Identification and verification of cell-type clusters with marker genes.

(A) Heatmap of top 10 marker genes in cell-type clusters.

(B) Violin plots of specific expression of representative marker genes in each cell type.

(C) Representative *in situ* hybridization of cell-type marker genes for the three putative clusters.

(t-distributed stochastic neighborhood embedding) software and the UMAP tool (Uniform Manifold Approximation and Projection), resulting in 13 clusters on the basis of comprehensive analyses of 8 samples under natural and salt-stressed conditions

(supplemental Excel 3; Figure 1B). PCC analysis was performed on the 13 clusters to help us annotate the cell types. Higher correlation coefficients were observed between cluster 4 and clusters 1, 9, and 12, between cluster 9 and clusters 4, 7, and 12, between cluster 8 and clusters 2 and 6, and between cluster 6 and cluster 8 (supplemental Figure 4A), indicating their potential closer connections with development and differentiation orders. Because abundant and accurate scRNA-seq information was available for root tissues of *A. thaliana* (Zhang et al., 2019a, 2019b), we also analyzed inter-species PCCs of root clusters between *A. thaliana* and *G. arboreum* (supplemental Figure S4B). The majority of pairwise group comparisons showed relatively low correlation coefficients, but correlation coefficients >40% were observed between clusters 4, 7, 9, 11, 12, and 13 of *G. arboreum* and the epidermis, lateral root cap, proximal meristem, and stem cell niche of *A. thaliana*. This comparison helped us to identify specific cell types in cotton roots, although there were some differences between cotton and *A. thaliana* scRNA-seq.

Identification and verification of cell-type clusters by *in situ* hybridization

First, the top 10 marker genes from 13 putative cell-type clusters were identified on the basis of their specific expression patterns and differential enrichment (Figure 2A; supplemental Excel 4); these were subsequently subjected to homologous alignment with the marker genes of *A. thaliana* roots (Zhang et al., 2019a, 2019b). The PsctH (<http://jinlab.hzau.edu.cn/PsctH/>) website (Xu et al., 2022) was used to search the enriched marker genes

from published scRNA-seq datasets (supplemental Excel 5), and these previous studies also helped us to predict the cell types. Finally, *in situ* RNA hybridization was performed on some representative marker genes from this study, and the major cell-type clusters were comprehensively identified as follows (Figure 1B and 1C): cluster 1 (root hair: 8318 cells), cluster 2 (epidermis: 7498 cells), cluster 3 (root cap: 7209 cells), cluster 4 (proximal meristem: 6804 cells), cluster 5 (cortex: 5574 cells), cluster 6 (xylem: 5483 cells), cluster 7 (quiescent center: 5034 cells), cluster 8 (endodermis: 4560 cells), cluster 9 (stem cell niche/meristem: 3393 cells), cluster 10 (endodermis: 1030 cells), cluster 11 (phloem: 834 cells), cluster 12 (cortex: 421 cells), and cluster 13 (xylem: 114 cells). Longitudinal and transverse structure diagrams of cotton lateral root tips were drawn on the basis of these identified cell types (Figure 1D).

For root hair cells, the representative marker gene *PME24* (*Ga06G2174*) was specifically expressed in cluster 1 (Figure 2B; supplemental Figure 5), and its homologous gene has been recognized as a marker gene for root hair cells in *A. thaliana* (Zhang et al., 2019a, 2019b; Shulse et al., 2019). Pectin methylesterases have been reported to participate in root hair development (Guénin et al., 2017; Cheong et al., 2019). Two other marker genes, *PER27* (*Ga03G1501*) and *AGP30* (*Ga10G0077*), were identified as marker genes of trichoblast cells in *A. thaliana* roots (Zhang et al., 2019a, 2019b; Shulse et al., 2019) and have been shown to be differentially or specifically expressed in root hairs (van Hengel et al., 2004; Wan et al., 2005).

For epidermal cells, the representative marker gene *GH3.6* (*Ga03G2153*) was found to be specifically expressed in cluster 2 (Figure 2B; supplemental Figure 6), and its homologous gene was identified as a marker gene of epidermal cells in the *Arabidopsis* root (Efroni et al., 2016; Zhang et al., 2019a,

2019b). One of the GRETCHEN HAGEN 3 (GH3) enzymes, namely GmGH3-14, has been observed to act primarily in the epidermal cells of legume roots (Damodaran et al., 2017), consistent with the result of *in situ* RNA hybridization of GH3.6 (Figure 2C). Another marker gene, *BAS1/CYP734A1* (Ga14G1953), has been identified as a marker gene of epidermal cells in *Arabidopsis* scRNA-seq data (Kim et al., 2021); this catabolism gene associated with brassinosteroi (BR) biosynthesis was significantly highly expressed in carrot roots (Que et al., 2017). The epidermis-specific marker gene *EP1* (Ga01G0569) was also specifically expressed in root epidermal cells; and expression of its homolog has been documented in carrot roots by *in situ* mRNA analysis (van Engelen et al., 1993).

For root cap cells, the representative marker gene *CYP88D6* (Ga08G1867) preferentially showed higher expression in cluster 3 (Figure 2B; supplemental Figure 7), and its homolog is also regarded as a specific marker gene of lateral root cap cells (Denyer et al., 2019; Wendrich et al., 2020). Previous studies have suggested that the participation of *CYP88D6* in glycyrrhizin biosynthesis is relevant not only to lateral root development (Zhang et al., 2022a, 2022b, 2022c) but also to the salt stress response (Wang et al., 2021a, 2021b, 2021c), and its specific expression in root cap cells has been observed by *in situ* RNA hybridization (Figure 2C). Another marker gene identified here, *BRN2* (Ga08G2713), has been recognized as a specific marker gene of root cap cells in *Arabidopsis* scRNA-seq data (Apelt et al., 2022) and was reported to regulate cellular maturation of the root cap in *Arabidopsis* (Bennett et al., 2010).

For proximal meristem cells, three marker genes were specifically expressed in cluster 4 (Figure 2B; supplemental Figure 8), *argC* (Ga10G1739), *UBC19* (Ga07G1357), and *Ga12G2480*, and their homologs have been identified as specific marker genes of proximal meristem cells in *Arabidopsis* roots (Zhang et al., 2019a, 2019b; Wendrich et al., 2020). Another top 10 marker gene, *Ga03G1871*, encodes dicer-like protein 2, which has been shown to participate in the regulation of root meristem activities by generating mobile small RNAs (Melnyk et al., 2011).

For cortex cells, the representative marker gene *NDR1* (Ga09G1539) was specifically expressed in clusters 5 and 12 (Figure 2B; supplemental Figure 9), and another representative marker gene, *C/VIF2* (Ga14G2368), was expressed specifically in cluster 12 (Figure 2B; supplemental Figure 10). A homologous *C/VIF2* gene has been recognized as a cortical cell marker in multiple scRNA-seq datasets (Denyer et al., 2019; Apelt et al., 2022; Shahan et al., 2022). Another three marker genes, *Ga05G0076* (AT4G30420), *Ga11G4095* (AT1G73620), and *Ga08G0823* (AT2G48020), have also been previously identified as cortical cell markers in *Arabidopsis* scRNA-seq studies (Denyer et al., 2019; Wendrich et al., 2020; Shahan et al., 2022).

For xylem cells, two representative marker genes, *ITPK3* (Ga14G1479) and *Ga06G0803*, were specifically expressed in clusters 6 and 13, respectively (Figure 2B; supplemental Figures 11 and 12). An *ITPK3* homolog has been recognized as a specific marker gene for xylem cells in the *Arabidopsis* root (Graeff et al., 2021). Another two marker genes, *GT-3A*

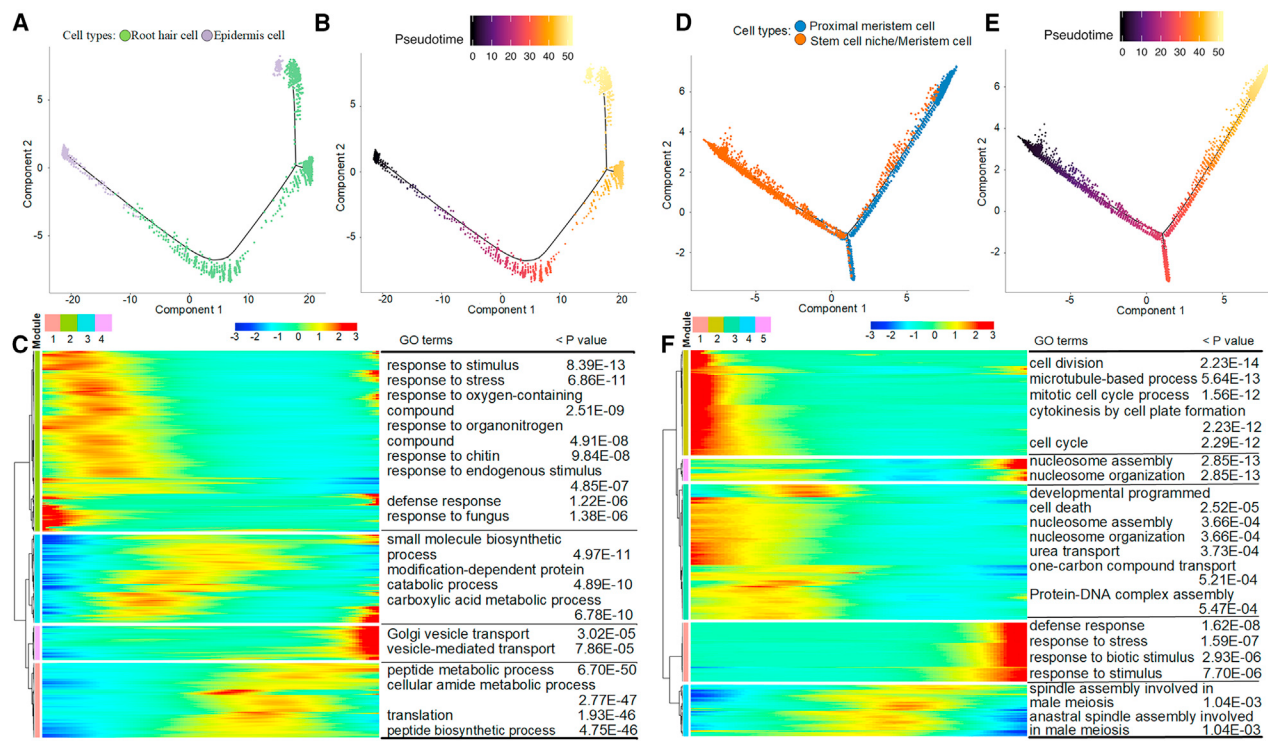
(Ga09G1979) in cluster 6 and *OPT7* (Ga08G1297) in cluster 13, have also been identified as xylem cell markers in previous work (Turco, 2019; Graeff et al., 2021). In addition, *MYB308* (Ga09G1898) was matched as a marker gene of xylem cells in *Arabidopsis* scRNA-seq datasets (Zhang et al., 2019a, 2019b; Turco et al., 2019), and its homolog *MYB46* (AT5G12870) has been shown to play important roles in xylem development (Xiao et al., 2021).

For quiescent center cells, the representative marker gene *COR47* (Ga12G2705) was specifically expressed in cluster 7 (Figure 2B; supplemental Figure 13), and its homolog has been recognized as a specific marker gene for late-stage meristemoid cells in *Arabidopsis* cotyledons (Liu et al., 2020). Homologs of *Nucleolin 2* (Ga01G0172) and *CBF5* (Ga01G0172) were identified as marker genes of quiescent center cells (Wendrich et al., 2020; Serrano-Ron et al., 2021), and *CMT3* (Ga07G0535) was recognized as a marker gene of quiescent center-like cells (Zhai and Xu, 2021).

For endodermal cells, the representative marker genes *Ga09G2354* and *MYB36* (Ga05G0063) were specifically expressed in clusters 8 and 10, respectively (Figure 2B; supplemental Figures 14 and 15), and their homologs have also been recognized as marker genes of endodermal cells in *Arabidopsis* scRNA-seq data (Zhang et al., 2019a, 2019b; Shulse et al., 2019). *MYB36* was reported to be important for the transition from proliferation to differentiation of *Arabidopsis* root endodermal cells (Liberman et al., 2015), and its specific expression was observed here in root cap cells by *in situ* RNA hybridization (Figure 2C). In addition, *XTH30* (Ga08G1818), *CYP81D1* (Ga12G2524), and *IRK1* (Ga08G0971) have previously been identified as marker genes of endodermal cells in *Arabidopsis* scRNA-seq studies (Jean-Baptiste et al., 2019; Turco et al., 2019; Graeff et al., 2021).

For meristem/stem cell niche cells, the representative marker gene *Histone H4* (Ga08G0060) was specifically expressed in cluster 9 (Figure 2B; supplemental Figure 16), and its homolog has been recognized as a marker gene for meristem cells in *Arabidopsis* scRNA-seq data (Turco et al., 2019; Shahan et al., 2022). Another two histone-related genes were also identified as marker genes in cluster 9, namely *Histone H3.2* (Ga08G2806) and *Histone H2AX* (Ga08G2166), which were separately identified as marker genes of early-stage and late-stage meristem cells in *Arabidopsis* scRNA-seq data (Liu et al., 2020). Previous studies have indicated that these histone-related genes not only function as epigenetic factors in root meristems (Kang et al., 2020) but also participate in stem cell niche maintenance during root development (Ma et al., 2018).

For phloem cells, the representative marker gene *Ga07G2664* was specifically expressed in cluster 11 (Figure 2B; supplemental Figure 17), and its homolog has been recognized as a marker gene for phloem cells in *Arabidopsis* scRNA-seq data (Zhang et al., 2019a, 2019b; Wendrich et al., 2020). *WAT7* (Ga06G0071) and *Ga11G4124*, selected as marker genes of cluster 11, were also identified as marker genes for phloem cells and phloem companion cells in multiple scRNA-seq datasets (Jean-Baptiste et al., 2019; Turco et al., 2019; Farmer et al., 2021).

**Figure 3. Differentiation trajectories and GO enrichment analysis of specific root cell types.**

(A and B) Differentiation process and pseudotime trajectory from epidermal to root hair cells. Each dot represents a single cell.

(C) Heatmap of branch-dependent genes clustered in epidermal and root hair cells over pseudotime analysis.

(D and E) Differentiation process and pseudotime trajectory from stem cell niche to proximal meristem cells.

(F) Heatmap of branch-dependent genes clustered in stem cell niche and proximal meristem cells over pseudotime analysis.

Differentiation trajectories of specific root cell types

Given the increasing evidence that the epidermis and root hairs have a close relationship (Liu et al., 2021a, 2021b, 2021c; Zhang et al., 2021a, 2021b), pseudotime analysis was used on these two cell types of the outermost root layer to confirm their differentiation order and developmental fate. Different cell types were separately clustered into two ends of the pseudotime backbone (Figure 3A), and the pseudotime trajectory represented by color depth helped us to pinpoint the beginning of the differentiation process (Figure 3B). Representative marker genes from the two cell types were also subjected to differentiation trajectory analyses, and *Ga01G0569*, *Ga03G2153*, and *Ga05G2041* of the epidermal cells, as well as *Ga03G1501*, *Ga06G2174*, and *Ga12G1149* of the root hair cells, showed the same differentiation patterns as whole single cells (supplemental Figure 18A–18F). In addition, the branch-dependent genes were used to perform heatmap analysis, which resulted in four different modules: modules 1 and 3 lay in the middle stages of the transition. Epidermis-related genes were mainly found in module 2, and root hair-related genes were mainly found in module 4. The genes in module 2 were significantly enriched in the GO terms response to stimulus (GO:0050896), response to stress (GO:0006950), and response to oxygen-containing compound (GO:1901700), consistent with the biological processes of root epidermal cells (Mochizuki et al., 2005; Bernhardt et al., 2005; Wang et al., 2020a, 2020b, 2020c). The genes in module 4 were significantly enriched in the GO terms Golgi vesicle transport (GO:0048193), vesicle-

mediated transport (GO:0016192), and single-organism intracellular transport (GO:1902582); the biological process of vesicle transport is reported to participate in root hair development and stress response (Lombardo and Lamattina, 2012; Kohli et al., 2022). Together, these results indicated that root hair cells were differentiated from epidermal cells.

Pseudotime analysis was also performed on the proximal meristem cells and stem cell niche/meristem cells to illustrate their differentiation trajectory, which has previously been analyzed by scRNA-seq of the *Arabidopsis* root (Zhang et al., 2019a, 2019b). Proximal meristem cells and stem cell niche/meristem cells were separately clustered at the two ends of the pseudotime backbone (Figure 3D), and their differentiation trajectory was represented by color depth (Figure 3E). Differentiation trajectory analyses on representative marker genes from the two cell types revealed that *Ga08G0060*, *Ga08G2166*, and *Ga08G2806* of the proximal meristem cells and *Ga07G1357*, *Ga10G1739*, and *Ga12G2480* of the stem cell niche/meristem cells showed the same differentiation patterns as whole single cells (supplemental Figure 18G–18L). The branch-dependent genes were used to perform heatmap analysis, resulting in five different modules based on expression levels (Figure 3F). Modules 1 and 2 were clearly situated at both ends of the differentiation trajectory, whereas modules 3–5 lay in the middle stages of the transition. The proximal meristem-related genes were found mainly in module 1, and the stem cell niche/meristem-related genes were found mainly in module 2.

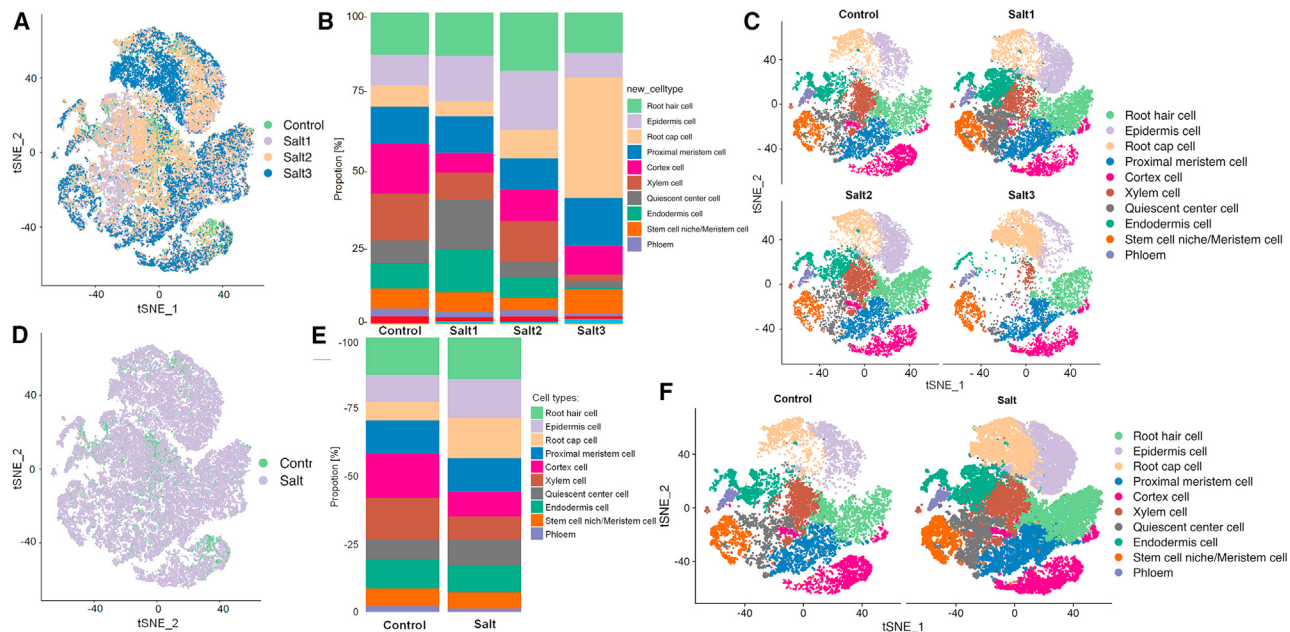


Figure 4. Variation in cell-type clusters in response to different salt stresses.

(A and B) t-SNE visualization and histogram of total acquired cells under natural growth conditions and three different salt stresses.

(C) Multi-dimension reduction clustering of different cell-type clusters under natural growth conditions and three different salt stresses.

(D and E) t-SNE visualization and histogram of total acquired cells under natural growth conditions and salt stress.

(F) Multi-dimension reduction clustering of different cell-type clusters under natural growth conditions and salt stress.

The genes in module 1 were significantly enriched in the GO biological process terms (BPs) cell division (GO:0051301) and mitotic cell-cycle process (GO:1903047), which have been reported to play important roles in proximal meristem cells to promote root development (Reddy et al., 2004; Takatsuka and Umeda, 2014; Zhang et al., 2022a, 2022b, 2022c; Li et al., 2022). The genes in module 2 were significantly enriched in the GO terms nucleosome assembly (GO:0006334), protein-DNA complex assembly (GO:0065004), and chromatin assembly (GO:0031497), which are closely related to histone activities that may influence cell fate in stem cell niche/meristem cells (Zhang et al., 2022a, 2022b, 2022c; Foroozani et al., 2022; Franklin et al., 2022). Together, the pseudotime trajectory, separate gene modules, and enriched GO terms led us to conclude that the proximal meristem differentiated from the stem cell niche.

Identification of specific root cell types relevant to salt stress

To identify the specific root cell types that respond to salt stress, we performed differential analysis of single cells from 10 cell types by comparing samples from natural growth conditions and various stress treatments (Figure 4). t-SNE visualization of total cells from the control, salt1, salt2, and salt3 samples (Figure 4A and 4C) showed clear differences in cell numbers and types, and a more intuitive histogram is shown in Figure 4B. Similar profiles for the root hair (cluster 1) and epidermal (cluster 2) cells indicated that low salt concentration increased the numbers of these two cell types to adapt to salt stress, even over an extended stress duration, whereas high salt concentration resulted in reduced cell counts. Opposite trends were observed in root cap (cluster 3) and cortex (cluster

5 and 12) cells. There were no apparent differences between natural growth conditions and low salinity stress, even over an extended stress duration. However, numbers of the two cell types increased under high salinity stress, implying their putative functions in response to salt stress. Unusual profiles were observed for the quiescent center (cluster 7) and endodermis (clusters 8 and 10). Cell numbers of the quiescent center initially increased at low salt concentrations, declined over the extended duration of low salt stress, but increased under high-salinity treatment. Continuous changes in cell numbers were observed in xylem cells (clusters 6 and 13), whereas cell numbers were relatively stable in the proximal meristem (cluster 4), stem cell niche/meristem (cluster 9), and phloem (cluster 11).

When the three salt stress-treated samples were combined into one salt sample for overall comparison with the control, less variation was observed with t-SNE visualization (Figure 4D and 4F). However, there were dramatic differences in relative cell numbers: marked increases in the proportion of root hair, epidermal, and root cap cells under salt stress, together with reductions in cortex, xylem, and endodermal cells (Figure 4E). The cell-type genes from these six specific cell types (supplemental Excel 6) were subjected to GO enrichment analysis, and more similar biological processes were significantly enriched among the three outermost cell layer types, as well as among the other three inner cell types (supplemental Figure 19; supplemental Excel 7). Two common GO terms were enriched in the cell-type genes from the root hair, epidermal, and root cap cells: response to stress (GO:0006950) and glucosamine-containing compound metabolic process (GO:1901071). These results suggest that the root surface could play important roles as the first barrier and site of

perception of external stresses (Lupo et al., 2022). The specific GO BPs significantly enriched in root hair cells were water transport (GO:0006833) and fluid transport (GO:0042044), whereas defense response (GO:0006952) and response to biotic stimulus (GO:0009607) were specifically enriched in epidermal and root cap cells. These results revealed the diverse patterns of different root cell types under salt stress, implying that plants might maintain natural growth and development by regulating water transport in root hair cells and defense responses in epidermal and root cap cells (Zhang et al., 2022a, 2022b, 2022c; Chambard et al., 2022; Rajendran and Kim, 2022; Wang et al., 2022). Nearly half of the top 25 GO terms were shared among the cell-type genes of the cortex, xylem, and endodermis cells. These included amide biosynthetic process (GO:0043604), translation (GO:0006412), and peptide biosynthetic process (GO:0043043), which have been reported to contribute to plant adaption to salt stress (Rehman et al., 2022). KEGG pathway analysis was also performed on the cell-type genes from these six specific cell types (supplemental Figure 20; supplemental Excel 8). Glutathione metabolism (ko00480) and biosynthesis of secondary metabolites (ko01110) were enriched in all six specific cell types, and these processes have been shown to have a close relationship to salt-stress resistance in plants (Cimini et al., 2022; Liu et al., 2022a, 2022b, 2022c, 2022d). Metabolic pathways (ko01100) and galactose metabolism (ko00052) were specifically enriched in cell-type genes of root hair, epidermal, and root cap cells, and ribosome (ko03010) and pentose phosphate pathway (ko00030) were specifically enriched in cell-type genes of cortex, xylem, and endodermis cells. These pathways have also been shown to participate in plant resistance to salt stress in previous studies (García-Caparrós et al., 2022; Chen et al., 2022; Huan et al., 2014; Wang et al., 2022).

Identification and enrichment analysis of DEGs in response to salt stress

We identified 750, 833, 488, 1520, 1173, and 777 DEGs from the following comparisons: control vs. salt1, control vs. salt2, salt1 vs. salt2, control vs. salt3, salt1 vs. salt3, and control vs. salt (supplemental Figure S21A; supplemental Excel 9). Further filtering of the DEGs using the criteria $P < 0.05$ and fold-change > 2.0 resulted in identification of 54, 48, 12, 195, 169, and 51 significant DEGs, respectively (supplemental Excel 10). Overall, this indicated that more DEGs participated in the plant root response to salt stress either by increasing the duration under the same salinity condition or by increasing the salinity concentration for the same duration. Functional enrichment analyses were performed on these filtered DEGs, and the common and specific GO and KEGG terms were summarized using two analysis strategies: (1) simultaneously comparing the pairwise groups of control vs. salt1, control vs. salt2, control vs. salt3, and control vs. salt (abbreviated as control vs. salts) and (2) simultaneously comparing the pairwise groups of salt1 vs. salt2 and salt1 vs. salt3 (abbreviated as salt1 vs. salt2/3). No common BPs were enriched among the top GO terms of the control vs. the salt treatments (supplemental Figure S21B; supplemental Excel 11), although plant-type primary cell wall biogenesis (GO:0009833), mitochondrial electron transport, NADH to ubiquinone (GO:0006120), and seed coat development

(GO:0010214) were commonly observed in control vs. salt1 and control vs. salt2, and defense response (GO:0006952), response to biotic stimulus (GO:0009607), and response to stress (GO:0006950) were similarly clustered among control vs. salt3, salt1 vs. salt3, and control vs. salts. All of these common biological processes have been reported to participate in the process of plant salt resistance (Meyer et al., 2009; Bu et al., 2019; Nanda et al., 2019; Chun et al., 2021; Kausar and Komatsu, 2022). In addition, methylammonium transmembrane transport (GO:0072489) and plastoquinone biosynthetic process (GO:0010236) were preferentially enriched in the control vs. salt1 comparison, and aminoglycan catabolic process (GO:0006026), chitin metabolic process (GO:0006030), metabolic process (GO:0008152), and biological process (GO:0008150) were enriched in the control vs. salt2 and salt1 vs. salt2 comparisons. Besides the common BPs defense response (GO:0006952) and response to biotic stimulus (GO:0009607), aminoglycan catabolic process (GO:0006026) was also preferentially enriched in the control vs. salt3 and control vs. salts comparisons. These results indicate that plants may respond to salt stress by regulating methylammonium transmembrane transport (GO:0072489) and the plastoquinone biosynthetic process (GO:0010236) during low salinity stress (Bu et al., 2019; Kolomeichuk et al., 2020). Subsequently, metabolic and catabolic processes related to aminoglycans and chitin may occur under a longer duration of low salinity stress (Vaghela et al., 2022), finally promoting defense and stress responses under high salinity treatment (Rajendran and Kim, 2022; Wang et al., 2022).

Only one common enriched KEGG pathway was found in the control vs. salt treatments (supplemental Figure S22; supplemental Excel 12), i.e., metabolic pathways (ko01100), which has typically been reported to participate in plant response to salt stresses (García-Caparrós et al., 2022). Phenylpropanoid biosynthesis (ko00940), oxidative phosphorylation (ko00190), and biosynthesis of secondary metabolites (ko01110) were commonly enriched in all comparisons except salt1 vs. salt2, and these KEGG pathways have been shown to make contributions to plant protection against salinity stress (Farhat et al., 2019; Jia et al., 2022; Sharma et al., 2022). Tyrosine metabolism (ko00350) was preferentially enriched in the control vs. salt1 comparison, and diterpenoid biosynthesis (ko00904) and selenocompound metabolism (ko00450) were enriched in the control vs. salt2 and salt1 vs. salt2 comparisons, respectively. Nitrogen metabolism (ko00910) and ubiquinone and other terpenoid-quinone biosynthesis (ko00130) were common KEGG pathways among the control vs. salt1, control vs. salt3, salt1 vs. salt3, and control vs. salts comparisons. Butanoate metabolism (ko00650) was preferentially enriched in control vs. salt3, and phenylalanine metabolism (ko00360) and tropane, piperidine, and pyridine alkaloid biosynthesis (ko00960) were preferentially enriched in salt1 vs. salt3 and control vs. salts, respectively. These results indicate that the metabolism of tyrosine, diterpenoids, and selenocompounds may help plant roots to adapt to low salinity stress (Zhou et al., 2017; Sheikhalipour et al., 2021), and phenylalanine metabolism and some secondary metabolites may contribute to plant protection against high salinity stress (Jia et al., 2022; Sharma et al., 2022). Genes associated with specifically enriched GO terms

and KEGG pathways have practical significance for precisely confirming the candidate factors involved in the molecular mechanisms of cotton root responses to salt stress.

Identification of common DEGs and TFs related to salt resistance

To identify potential candidate genes that control the response of plant roots to salt stress, we performed multiple pairwise comparisons of all the control and salinity treatments (control-salt1-salt2-salt3). Although no common DEGs were identified among the multiple pairwise comparisons (Figure 5A), all the DEGs were subsequently combined and subjected to enrichment analyses. In the GO enrichment analysis (Figure 5C), defense response (GO:0006952), aminoglycan catabolic process (GO:0006026), and chitin metabolic process (GO:0006032) were the most enriched BPs, and chitinase activity (GO:0004568), peroxidase activity (GO:0004601), and oxidoreductase activity (GO:0016491) were the top 3 molecular function terms. These specifically enriched GO terms suggest that defense response, chitin catabolic/metabolic processes, and peroxidase or oxidoreductase activities may contribute to plant salt-stress resistance (Espinoza et al., 2017; Chun et al., 2021; Hashemipetroudi et al., 2022). Two of the DEGs associated with catabolism and metabolic processes of aminoglycans, chitin, amino sugars, and glucosamine-containing compounds were identified as *Ga08G1124* (annotated as hevamine-A-like) and *Ga11G2948* (chitinase 10), implying that they have potential functions in plant protection against salt stress (Wei et al., 2022; Vaghela et al., 2022). Ten enriched KEGG pathways were identified (Figure 6C), among which metabolic pathways (ko01100), biosynthesis of secondary metabolites (ko01110), and phenylpropanoid biosynthesis (ko00940) were the most significantly enriched. The three most frequently enriched DEGs, *Ga14G0244* (Major pollen allergen Bet v 1-F/I), *Ga10G1189* (peroxidase 24-like), and *Ga03G2286* (bacterial-induced peroxidase), were associated with the above-mentioned KEGG terms; the former was also annotated with the GO terms defense response (GO:0006952) and response to biotic stimulus (GO:0009607), and the latter two were annotated with the GO terms peroxidase activity (GO:0004601), response to oxidative stress (GO:0006979), hydrogen peroxide catabolic process (GO:0042744), and metal ion binding (GO:0046872) (Fujita and Inui, 2021; Coccozza et al., 2022).

Eight types of TFs were among the DEGs identified as important by pairwise comparisons between samples (supplemental Table 2; supplemental Excel 13), and C2H2, NAC, and WRKY TFs were the most abundant TFs in response to salt stress. Multiple comparisons were performed to identify the common TFs, and there were no common TFs in control-salt1-salt2-salt3 (Figure 5B). Nonetheless, some patterns were apparent. Almost no TF DEGs were found under the low salinity treatments, with the exception of *Ga05G1262* (WRKY TF 40-like) in control vs. salt2. Novel TF types and more TFs were observed at the higher salt concentration: bHLH, MYB, NAC, WRKY, and bZIP were the common TF types always present in control vs. salt3 and salt1 vs. salt3; and only one bHLH in control vs. salt3 while two AP2/ERF-ERF and one Tify TF types salt1 vs. salt3 were separately identified. In general, more TF types participated in defense against higher salinity concentration, and C2H2, MYB, NAC, WRKY,

and bZIP TFs played key roles in the response to salt stress as common TFs (Pan et al., 2017; Gao et al., 2020; Yu et al., 2020; Wang et al., 2021a, 2021b, 2021c). Some specific TFs were also identified, such as bHLH, AP2/ERF-ERF, and Tify from the control vs. salt3 and salt1 vs. salt3 comparisons (Wu et al., 2015; Sun et al., 2018; Debbarma et al., 2019). GO enrichment analysis of total TFs (Figure 5D) indicated that most of the TF genes were associated with regulation of transcription, DNA-templated (GO:0006335), regulation of nucleic acid-templated transcription (GO:1903506), and regulation of RNA biosynthetic process (GO:2001141), consistent their biological functions (Verma et al., 2022). All TFs were enriched in the specific KEGG pathway of plant hormone signal transduction (ko04075), and only one associated DEG *Ga01G0229* has been reported to participate in plant hormone signal transduction in response to JA (Ye et al., 2022). These data provide abundant candidate genes for subsequent research on cellular heterogeneity verification and molecular mechanisms of plant salt stress response.

Hormone biosynthesis and response profiles in root tips under salt stress

Phytohormones play vital roles in regulation of the plant life cycle under both natural growth and stress conditions (Yu et al., 2020), and we therefore comprehensively analyzed the responses of hormone-related DEGs to salt stress to investigate hormone biosynthesis and response patterns in specific cell types (Figure 6; supplemental Excel 14). DEGs associated with seven hormone types were identified in this study: 24, 9, 45, 20, 3, 16, and 2 DEGs associated with auxin, cytokinin, ABA, ethylene, gibberellic acid (GA), JA, and BR, respectively. Overall, the majority of plant hormone-associated DEGs were associated with epidermal, root cap, xylem, and endodermal cell types and were related to auxin, cytokinin, ABA, ethylene, and JA. Auxin-related genes included three marker genes, *Ga03G2153* (epidermal cells), *Ga12G1669* (xylem cells), and *Ga13G1932* (endodermal cells), and ABA-related genes included the marker gene *Ga12G2863* (xylem cells). Among these four marker genes, *Ga12G1669* encodes a WRKY TF that has been reported to improve plant salt-stress resistance by mediating auxin signal transduction (Singh et al., 2023), and the auxin-related *Ga13G1932* has been reported to participate in glutathione metabolism (Cimini et al., 2022). The GA-related and BR-related DEGs were enriched in cortical cells, where their specific expression might be important for corresponding reactions to salt stress (Song et al., 2022; Velandia et al., 2022). The reason why some hormone-related DEGs were found in multiple cell types was that these relatively non-specific DEGs had homogeneous expression patterns in different cell populations.

Silencing of *GH3.6* in *G. arboreum* affects plant morphology and physiology

The common DEG *Ga03G2153* (*GH3.6*) was not only annotated as a marker gene for epidermal cells but also reportedly responsive to auxin signal transduction. We therefore performed a virus-induced gene silencing (VIGS) experiment to verify its function under salt stress. When NaCl stress (200 mM) was applied to wild-type (WT), unloaded (TRV:00), and *GaGH3.6*-silenced (TRV:*GaGH3.6*) SXY-1 plants, we observed more pronounced leaf wilting in the *GaGH3.6*-silenced plants (Figure 7A).

Plant Communications

Transcriptional landscape of cotton roots

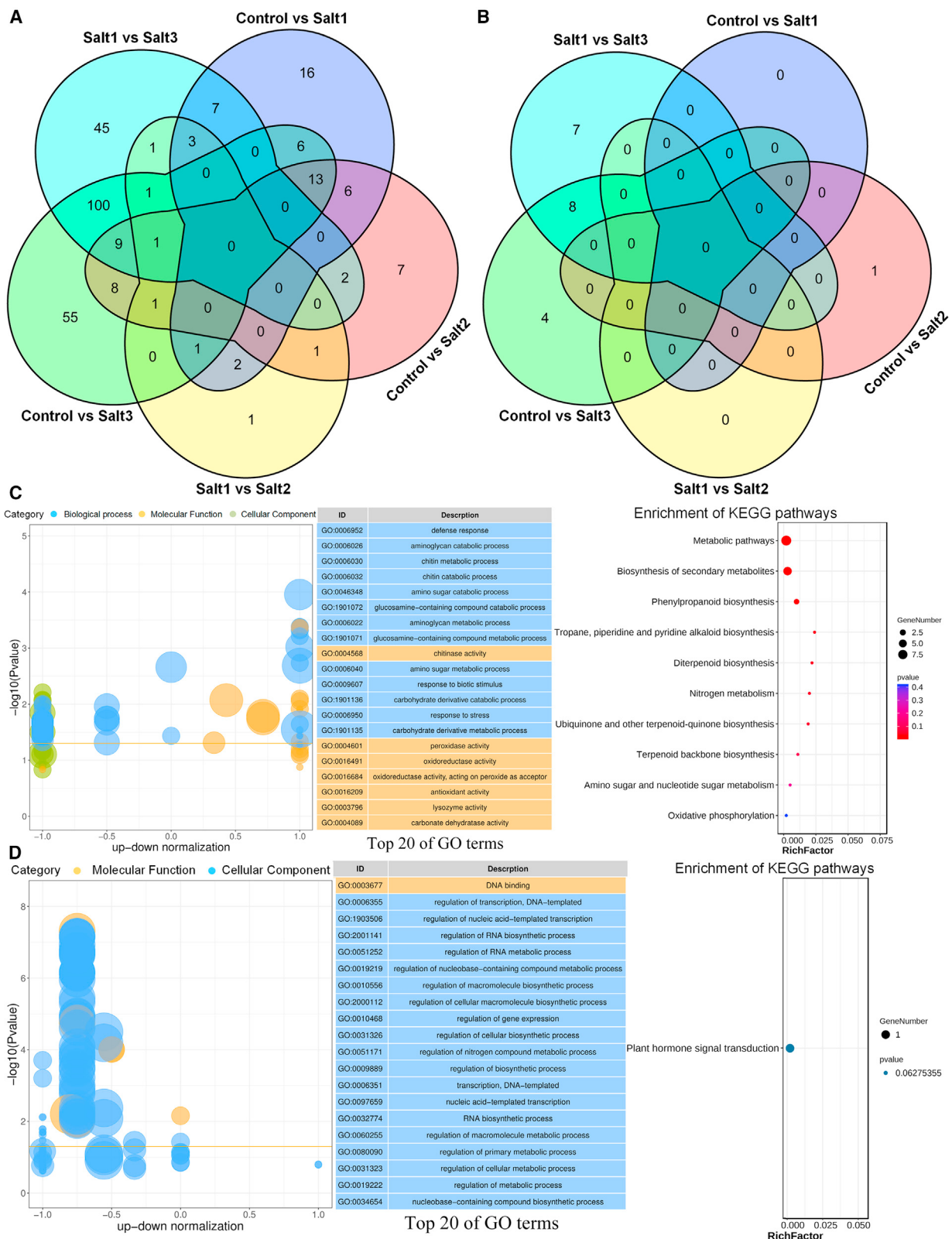


Figure 5. Identification of common DEGs and TFs related to salt resistance.

(A and B) Venn diagram of common identified DEGs and TFs under multiple salt stresses.

(C) GO enrichment and KEGG pathway analyses of common DEGs under different salinity levels for the same duration.

(D) GO enrichment and KEGG pathway analyses of total TFs.

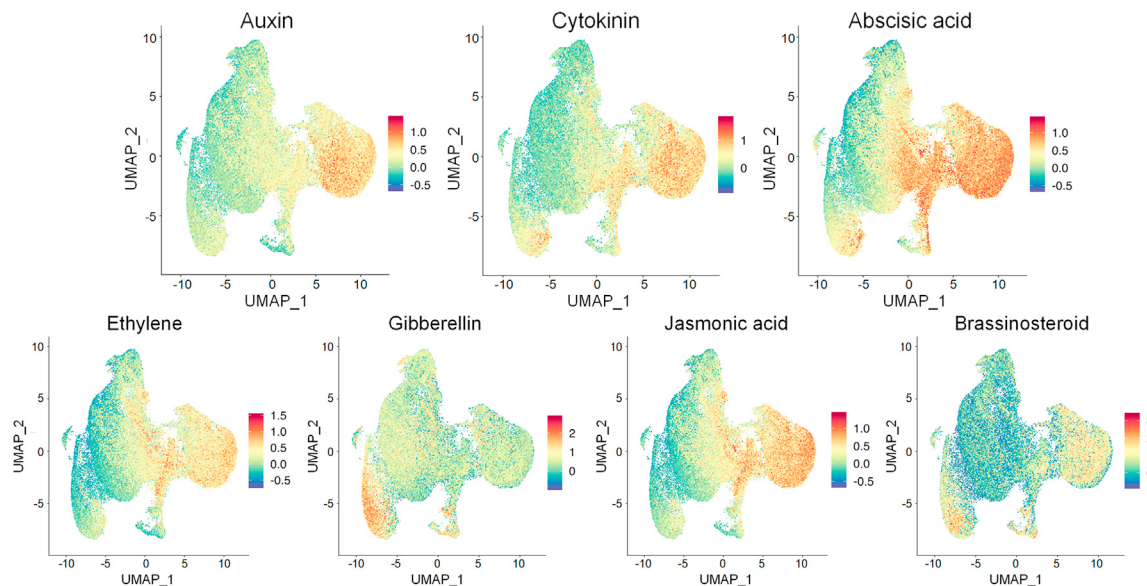


Figure 6. UMAP visualization of expression patterns of DEGs associated with plant hormones in response to salt stress.

Silencing efficiency was calculated by qRT-PCR, and significant differences in relative expression of *GaGH3.6* among WT, TRV:00, and TRV:*GaGH3.6* plants (Figure 7B) confirmed that the stress susceptibility phenotype resulted from *GaGH3.6* silencing.

We also evaluated oxidative stress damage in leaves by DAB staining and ion leakage measurements. There was no staining or significant difference among WT, unloaded, and TRV:*GaGH3.6* leaves before 200 mM NaCl treatment (Figure 7C), indicating no accumulation of hydrogen peroxide. Brown substances were produced in leaves of WT, unloaded, and TRV:*GaGH3.6* plants after salt treatment, and their levels were highest in *GaGH3.6*-silenced leaves, implying more severe oxidative stress. Salt stress also caused increases in leaf ion leakage, and ion leakage was significantly higher in *GaGH3.6*-silenced leaves, indicating that their mesophyll cells were more seriously damaged by oxidative stress (Figure 7D). No significant differences were observed in chlorophyll content and relative leaf water content (RLWC) among the three materials before

NaCl treatment (Figures 7E and 7F). These parameters declined in all genotypes under salt stress but were significantly lower in *GaGH3.6*-silenced leaves than in WT and TRV:00 leaves. These findings suggest that silencing of *GaGH3.6* compromised plant tolerance to salt stress.

DISCUSSION

Soil salinization is widespread around the world and is one of the most serious abiotic stresses affecting plant growth and development. It reduces both yield and quality and has gradually become a major threat to global food security (Zhang et al., 2020). Plants have developed highly efficient and accurate regulatory networks for adaptation to salt stress, and many crucial signaling pathways and key functional genes have been identified through numerous transcriptome and other molecular biology studies on different varieties, tissues, and salt stresses (Gong et al., 2020). As one

of the most commonly used techniques to investigate specific biological processes, bulk RNA-seq is still constrained by the fact that it obscures cell heterogeneity, and this has become the major driving force for the emergence of scRNA-seq, which can reveal cell fate selection and organogenesis with a higher degree of resolution (Wen and Tang, 2022). In recent years, transcriptome landscapes at a single-cell resolution have been constructed for a large number of model and non-model plants, including herbs, woody plants, food crops, cash crops, and vegetable crops. Fewer such studies have been performed under stress conditions, perhaps because of difficulties in isolating high-quality protoplasts that meet the requirements for single-cell sequencing. This prompted us to consider a number of factors, including root age, enzyme composition, zymolytic duration, vacuum treatment time, and duration and concentration of salinity, and ultimately enabled us to develop an optimized method of protoplast dissociation suitable for cotton lateral root tips (Liu et al., 2022a, 2022b, 2022c, 2022d). The use of vacuum treatment not only helped to reduce dissociation time but also, more significantly, ensured that a wide variety of cell types could be obtained, thus helping us to identify 13 cell-type clusters from 61 095 single cells through scRNA-seq (Figure 1A).

The top 10 identified marker genes were subjected to homologous alignment (Zhang et al., 2019a, 2019b), PsctH database searching (Xu et al., 2022), and comparison with previous studies, ultimately confirming the accuracy of 10 cell types in clusters 1 to 13 (Figure 1B and 1C). In general, cells of external cell types were more numerous than those of inner cell types, consistent with progress of dissociation from outside to inside and indirectly confirming the accuracy of our scRNA-seq data. We performed *in situ* RNA hybridization verification for three representative marker genes, *Ga03G2153* (epidermis), *Ga08G1867* (root cap), and *Ga05G0063* (endodermis), and the RNA FISH results coincided with the predictions based on comprehensive bioinformatics analyses (Figure 2D). Because root hair cells differentiate from epidermal cells (Liu et al., 2021a, 2021b,

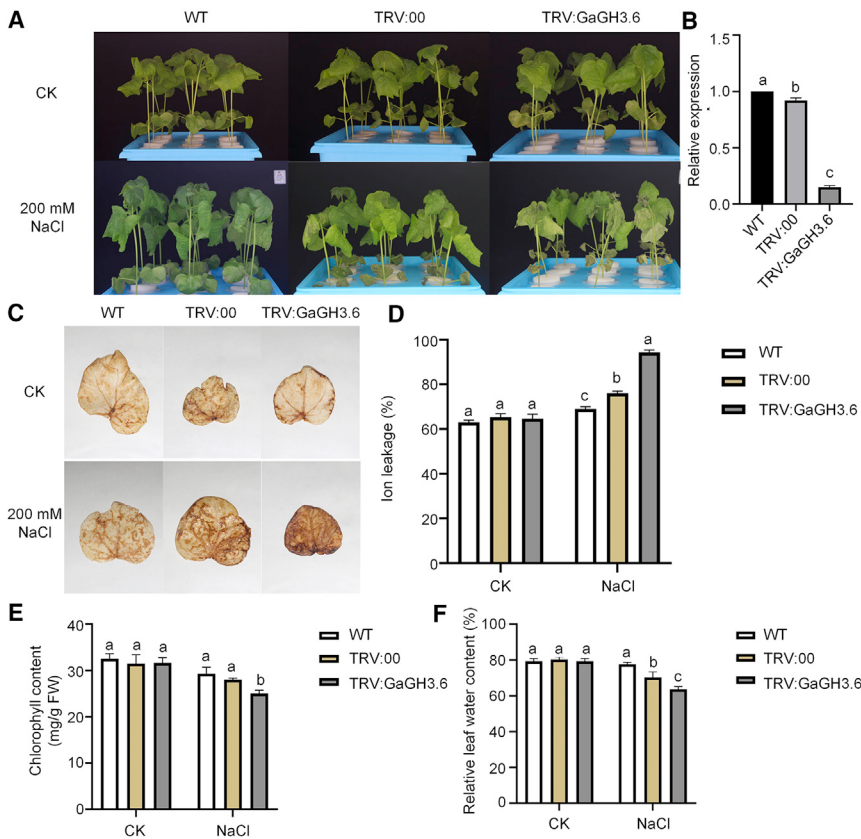


Figure 7. Virus-induced gene silencing of *GaGH3.6* and phenotype evaluation

(A) WT, TRV:00, and TRV:GaGH3.6 seedlings grown in hydroponics under natural growth conditions and 200 mM NaCl treatment.

(B) Relative expression (three biological replicates, $n = 3$) of *GaGH3.6* in WT, TRV:00, and TRV:GaGH3.6 seedlings.

(C and D) DAB staining and ion leakage ($n = 3$) of cotton leaves from WT, TRV:00, and TRV:GaGH3.6 plants under CK and 200 mM NaCl conditions.

(E and F) Chlorophyll content ($n = 10$) and relative leaf water content ($n = 3$) of cotton leaves under CK and 200 mM NaCl conditions. Different letters above the bars represent the same sample comparisons under CK and 200 mM NaCl; a, b, and c indicate the none ($P > 0.5$), existing ($P < 0.5$), and significant differences ($P < 0.01$). Error bars represent standard deviations of biological replicates.

2021c), their differentiation trajectory was predicted by pseudotime analysis (Figure 3A and 3B). GO enrichment analyses of branch-dependent genes (Figure 3C) revealed enriched biological processes that pointed to terminal or middle cell states, and the differentiation relationship between the epidermis and root hair cells was also substantiated (Zhang et al., 2021a, 2021b). Pseudotime analysis was also performed to reveal the differentiation trajectory of the proximal meristem and the stem cell niche (Figure 3D and 3E), and the results were consistent with those of *Arabidopsis* root scRNA-seq data (Zhang et al., 2019a, 2019b).

Accurate information for specific cell types is the basis for differential analysis of their responses to salt stress, and various cell types showed corresponding variations under salt stress. To detect the patterns or most variable root cell types, we performed multiple salt-stress comparisons and integrated salt-stress samples with natural-growth samples, ultimately identifying dramatic increases in the numbers of root hair, epidermal, and root cap cells and reductions in cortex, xylem, and endodermal cells of salt-treated samples (Figure 4B and 4E). The GO terms response to stress (GO:0006950) and glucosamine-containing compound metabolic process (GO:1901071) were commonly enriched in cell types of the three outermost cell layers, implying the significance of the root surface for protecting plants from stress (Lupo et al., 2022). Specific enriched GO terms were separately identified in different cell types, and the results indicated that the root hair, epidermal, and root cap cells might adapt to salt stress by regulating water transport (GO:0006833) and fluid transport (GO:0042044) in epidermal cells and by initiating

defense responses (GO:0006952) and responses to biotic stimulus (GO:0009607) in the epidermal and root cap cells (Zhang et al., 2022a, 2022b, 2022c; Chambard et al., 2022; Rajendran and Kim, 2022; Wang et al., 2022). More common GO terms were enriched in cell-type-specific genes of cortex, xylem, and endodermal cells compared with those of root

hair, epidermal, and root cap cells, and these included amide biosynthetic process (GO:0043604), translation (GO:0006412), and peptide biosynthetic process (GO:0043043), which have been shown to promote plant resistance to salt stress (Rehman et al., 2022). Some important KEGG pathways were identified, including glutathione metabolism (ko00480), biosynthesis of secondary metabolites (ko01110), metabolic pathways (ko01100), galactose metabolism (ko00052), ribosome (ko03010), and pentose phosphate pathway (ko00030), all of which have been reported to play significant roles in maintaining the natural growth of plants (Garcia-Caparrós et al., 2022; Chen et al., 2022; Huan et al., 2014; Wang et al., 2022). We expected that more epidermal cells might differentiate into root hairs under salt stress, and this hypothesis was confirmed by a slight increase in the cell numbers of root hairs, which, combined with root cap and epidermal cells, would enhance the root surface for water and nutrient acquisition in response to stress (Arif et al., 2019). Fewer endodermal cells might result from fewer meristem cells, as the former differentiate into the latter, which subsequently form Caspary strips and undergo suberization (White, 2001). Absence or reduction of suberin could help ions and water move more easily across the endodermis, facilitating the transport of more Na^+ into the water column and, ultimately, the leaf blade. By contrast, more K^+ could be stored, and limited water backflow may promote higher salt tolerance in plants (Wang et al., 2020a, 2020b, 2020c, 2020d, 2020e). Despite the relatively short processing time under salt stress, subsequent protoplast dissociation was performed for almost 6 h, during which time the mannitol treatment caused the same osmotic stress on the

lateral root tips as that brought about by salt stress (Zhu 2016). The long duration of osmotic stress may be the predominant reason why there were dramatic changes in cell numbers at the single-cell resolution, although this might also result from some other objective factors. Additional *in situ* hybridization and genetic transformation experiments are needed to reveal the molecular mechanism.

Common enriched subcategories were identified by pairwise comparisons between samples (supplemental Figure S21), and plant-type primary cell wall biogenesis (GO:0009833), mitochondrial electron transport, NADH to ubiquinone (GO:0006120), defense response (GO:0006952), response to biotic stimulus (GO:0009607), response to stress (GO:0006950), aminoglycan catabolic process (GO:0006026), and chitin metabolic process (GO:0006030) have previously been shown to participate in plant response to salt stress (Meyer et al., 2009; Bu et al., 2019; Vaghela et al., 2022; Nanda et al., 2019; Chun et al., 2021; Kausar and Komatsu, 2022; Rajendran and Kim, 2022; Wang et al., 2022). In the comparison group of control-salt1-salts, methylammonium transmembrane transport (GO:0072489) and plastoquinone biosynthetic process (GO:0010236) were separately enriched in the initial periods, suggesting their respective functions in adaptation to low salinity stress (Bu et al., 2019; Kolomeichuk et al., 2020). With the increased duration of low salinity stress, metabolic and catabolic processes related to aminoglycans and chitin contributed to plant adaptability to salt stress (Vaghela et al., 2022), finally promoting defense and stress responses under high salinity treatment (Rajendran and Kim, 2022; Wang et al., 2022). KEGG pathway enrichment results also revealed that phenylpropanoid biosynthesis (ko00940), oxidative phosphorylation (ko00190), and biosynthesis of secondary metabolites (ko01110) might protect plant roots against the influence of salt (Farhat et al., 2019; Jia et al., 2022; Sharma et al., 2022), together with glutathione metabolism (ko00480). Tyrosine, diterpenoid, and selenocompound metabolism might also help plant roots adapt to low salinity treatment (Zhou et al., 2017; Sheikhalipour et al., 2021), and phenylalanine metabolism and some secondary metabolites may make contributions to protecting plants against high salinity stress (Jia et al., 2022; Sharma et al., 2022). These findings provide significant information about additional screening factors that can balance plant growth and salt tolerance and also reveal the molecular mechanisms of plant root responses to salt stress at a more detailed level.

Revealing the molecular mechanisms of plant salt-stress resistance is necessary for identification of important functional genes. Only one common DEG (*Ga10G2451*) had GO enrichment and Pfam index among multiple pairwise comparisons (Figure 5A); it is regarded as an ABA-responsive gene that participates in salt tolerance in transgenic rice plants (Huang et al., 2018). Another common significant candidate gene (*Ga03G2153*, annotated as indole-3-acetic acid-amido synthetase GH3.6-like protein) was associated with the terms response to auxin (GO:0009507) and auxin-activated signaling pathway (GO:0009733), and it was verified by *in situ* hybridization as one of the top 10 marker genes of epidermal cells. In addition, other common DEGs related to alpha-linolenic acid metabolism, phenylpropanoid biosynthesis, and catabolic and metabolic processes of aminoglycans, chitin, amino sugars,

and glucosamine-containing compounds have been shown to participate in salt-resistance biological processes of plants (Yang et al., 2022; Jia et al., 2022; Wei et al., 2022; Vaghela et al., 2022). Eight types of TFs that responded to salt stress were identified in this study, including C2H2, NAC, WRKY, and other major TF families (Debbarma et al., 2019; Yu et al., 2020; Wang et al., 2021a, 2021b, 2021c), although no common TFs were identified from similar multiple comparisons (Figure 5B). There were apparent changes in the number of salt-responsive TFs as the salt-stress process advanced, and one Tify TF (*Ga01G0229*) was previously reported to participate in plant hormone signal transduction in response to JA (Ye et al., 2022). These gene resources should be combined with forward genetic data for further functional verification by genetic transformation and genome-editing technology.

Plants struggle to balance natural growth with stress responses during their whole life cycle. Hormones are important regulators of biological processes, and we therefore investigated their biosynthesis and response patterns in roots under salt stress (Figure 6). We identified DEGs associated with seven types of phytohormones by pairwise comparisons between different salinity treatments; most were associated with ABA and were preferentially enriched in epidermal, xylem, and endodermal cells, suggesting that this hormone has close relationships with these root cell types (Jin et al., 2022; Lu et al., 2022; Zhao et al., 2022). The unique marker gene of xylem cells was also identified as *Ga12G2863*, which is related to ABA. Next most abundant were auxin-related DEGs, which were principally enriched in epidermal, root cap, xylem, and endodermal cells. Three marker genes were identified as *Ga03G2153* (epidermal cells), *Ga12G1669* (xylem cells), and *Ga13G1932* (endodermal cells); the latter two DEGs were separately annotated as a WRKY TF and a glutathione-related factor involved in mediating auxin signal transduction (Sigh et al., 2023; Cimini et al., 2022). Interestingly, a marker gene participating in phytohormone biosynthesis was an auxin-related gene (*Ga03G2153*), and this candidate DEG, which was verified by *in situ* hybridization, was once more identified in this study, implying its potential significance for the plant response to salt stress. Cytokinin-related DEGs were clustered into xylem and root cap cells, and root cytokinin has been found to be synthesized in the root cap and exported through the xylem into young shoots via the transpiration stream (Aloni et al., 2005). JA-related DEGs were clustered into root cap, epidermal, xylem, and endodermal cells, whereas GA-related and BR-related DEGs were clustered into cortex cells, all of which have been reported to participate in root growth (Michelet et al., 2012; Ishimaru et al., 2018; Song et al., 2022; Velandia et al., 2022). Overall, these data provide significant information on phytohormone changes in response to salt stress from a single-cell perspective and also contribute to more precise applications of exogenous hormones in specific tissues for high-efficiency production.

Given its potential function in salt tolerance, the epidermal marker, auxin-related gene, and common DEG *GaGH3.6* was selected for VIGS verification, and the albino phenotype of the plant leaves confirmed the validity of the silencing system.

Compared with normal growth conditions in half-strength Hoagland nutrient solution, 200 mM NaCl treatment caused wilting symptoms in WT, TRV:00, and RTV:GaGH3.6 seedlings, but the degree of leaf wilting was significantly greater in the GaGH3.6-silenced RTV:GaGH3.6 (Figure 7). Stress typically causes changes in the ROS balance, resulting in oxidative stress and damage caused by ROS accumulation (Abbasi et al., 2007; Liu et al., 2022a, 2022b, 2022c, 2022d). 3,3'-N-Diaminobenzidine is a common dye used to detect the degree of oxidative damage in plants, as it loses electrons in the presence of hydrogen peroxide and forms brown insoluble products that accumulate to different levels in plant tissues (Shiraku et al., 2021). No staining was observed under normal conditions, and the greatest accumulation of brown substances was found in leaves of GaGH3.6-silenced plants, indicating that they experienced the most severe oxidative stress. Ion leakage is also an indicator of mesophyll cells responding to oxidative damage, and a significant increase was observed in GaGH3.6-silenced leaves under 200 mM NaCl treatment, implying that they were most seriously damaged by oxidative stress. These findings suggest that the candidate gene GaGH3.6 may participate in cotton salt tolerance and may also be involved in redox processes for maintaining ROS homeostasis under salt stress. In summary, scRNA-seq provides not only an unprecedented atlas of single-cell transcription with heterogeneity but also a more efficient and accurate strategy for identification of candidate genes.

METHODS

Plant growth and protoplast dissociation under natural and salt-stress conditions

After sterilization with 0.1% HgCl₂ for 15 min, mature seeds of *G. arboreum* SXY1 were rinsed at least three times with deionized water and germinated on 1/2 Murashige and Skoog (MS) solid medium with 15 g glucose and 2.6 g/L phytagel, adjusted to pH 5.7, and grown in an illumination incubator at 28°C/light for 16 h and 25°C/dark for 8 h. Subsequently, 5-day-old cotton seedlings were uniformly collected and randomly separated into four groups, which were immersed into 40 ml MS liquid medium for 0.5 h (natural growth control), MS liquid medium with 100 mM NaCl for 0.5 h (salt1) or 1 h (salt2), or 150 mM NaCl solution for 0.5 h (salt3). Two biological replications were performed to ensure the statistical significance of the study, and numerous lateral roots were separately collected for protoplast dissociation.

We developed an optimized method of protoplast dissociation suitable for cotton lateral root tips after comprehensive consideration of root age, enzyme composition, zymolytic duration, vacuum treatment time, and salt-stress influence factors (Liu et al., 2022a, 2022b, 2022c, 2022d). Lateral root tips (0.5–1 cm) were cut into pieces with a sharp blade and placed in a six-well cell culture dish containing 10 ml zymolytic solution (1.5% cellulase R10, 1% pectolyase, 0.4 M mannitol, 0.1 M KCl, 0.08 M MES, 0.02 M CaCl₂, and 0.1% BSA). Vacuum treatment (0.05 MPa) was performed in the dark for 1 h, and the enzymatic hydrolysis reaction lasted for about 6 h in a constant-temperature shaker with a gentle speed of 80 rpm at 25°C. A 40-μm cell strainer was used to filter the dissociated protoplasts. The protoplasts were collected by centrifugation and washed 2–4 times with WB buffer (0.1 M KCl, 0.08 M MES, 0.4 M mannitol, and 0.1% BSA) on standby. Finally, a hemocytometer was used to count the protoplasts, and staining with trypan blue and fluorescein diacetate was used to confirm their viability and fragmentation rate. The dissociated protoplasts satisfied scRNA-seq standards for quantity and quality, as captured by microfluidic technology of the 10x Genomics Single Cell Protocol (CG00052, RevC).

scRNA-seq library construction and sequencing

The 10x Genomics 3' Single Cell Platform was used to process the high-quality protoplasts according to the corresponding instructions, and single-cell gel beads in emulsions (GEMs) were generated by a microfluidic chip in different lanes. The scRNA-seq library was then constructed using Chromium Next GEM Single Cell 3' Reagent Kits v3.1 (10x Genomics, Pleasanton, CA). The quality of the DNA libraries was confirmed with an Agilent 2100 Bioanalyzer, and Illumina NovaSeq 6000 sequencing was performed on the eight samples with two biological replications.

Preprocessing of scRNA-seq data

Multiple alignments were performed between the raw scRNA-seq data obtained from eight samples and the *G. arboreum* reference genome (Du et al., 2018) and its mitochondrial genome (Chen et al., 2017) using the Cell Ranger software pipeline v5.0.0 (10x Genomics). A matrix of gene counts vs. cells was produced from normalized aggregate data across samples. The R package Seurat v3.1.2 (Butler et al., 2018) was used to process the unique molecular identifier counts matrix, and unique molecular identifier/gene number out of the limit of mean value ± two-fold of standard deviations was set as the filtering criteria for discarding doublets, unbound or apoptotic cells, and other unbound or low-quality cells and possible multiple captures. Total single cells were subjected to QC filtering to generate high-quality cells for further bioinformatic analyses using the stringent criteria of less than 5% mitochondria genes and less than 2% enzymatic hydrolysis genes. The NormalizeData function of Seurat (Butler et al., 2018) was used for library size normalization to obtain normalized counts. Specifically, “LogNormalize” was used as the global-scaling normalization method to normalize the gene expression measurements for each cell by the total expression and multiply them by a scaling factor (10 000 by default), ensuring that the results were log-transformed. The sequencing and bioinformatics analysis were performed by OE Biotech (Shanghai, China).

Cell clustering and marker gene identification

Top variable genes were identified by the genome-wide expression profiling method across single cells (Macosko et al., 2015), and the genes with the most variable expression were identified using FindVariableGenes (mean.function = FastExpMean, dispersion.function = FastLogVMR) in Seurat (Butler et al., 2018). With reference to the method of screening cell-cycle proteins in scRNA-seq data from the *Arabidopsis* vegetative shoot apex (Zhang et al., 2021a, 2021b), root spatiotemporal and gene expression maps (Birnbaum et al., 2003; Brady et al., 2007; Gutierrez, 2009) were also combined to search their homologous genes in cotton, resulting in a total of 74 genes relevant to cell-cycle proteins (supplemental Excel 1). It is particularly necessary to point out that only the two bulk RNA-seq results from natural growth conditions were subjected to comparison analyses before and after protoplast dissociation to identify genes and their related GO enrichment and KEGG pathways associated with enzymatic hydrolysis (Liu et al., 2022a, 2022b, 2022c, 2022d), helping us to identify genes only affected by enzymatic hydrolysis while removing the influence of salt stress. Finally, 300 genes were identified as participating in the enzymatic hydrolysis reaction (supplemental Excel 2) and were used for eliminating the effects on subsequent gene analysis. To reduce the dimensionality and cluster the single cells on the basis of their gene expression profiles, principal-component analysis and graph-based clustering were performed separately with the RunPCA function and FindClusters function in Seurat (Butler et al., 2018). To remove batch effects in the scRNA-seq data, the mutual nearest neighbors approach was performed with the R package “batchelor” (Haghverdi et al., 2018). t-SNE arithmetic was used for cell visualization with the RunTSNE function in Seurat (Butler et al., 2018) and was simultaneously confirmed by Uniform Manifold Approximation and Projection software (Becht et al., 2018). The FindAllMarkers function (test.use = bimod) in Seurat (Butler et al., 2018) was used for marker gene identification, which also contributed to the

comparison with marker genes among all cell-type clusters for positive marker gene identification.

Pseudotime analysis

The differentiation trajectories of root cell types were analyzed with Monocle 2 (Trapnell et al., 2014) to investigate their pseudotime relationships. First, the importCDS (object, import_all = F) function was used to convert raw counts into the CellDataSet. The estimateSizeFactors () and estimateDispersions () functions of Monocle 2 (Trapnell et al., 2014) were then used to pre-calculate some important parameters related to the data, and the differentialGeneTest function package was used to select ordering genes (qval < 0.01) that were likely to be informative for the ordering of cells along the pseudotime trajectory. The ordered DEGs were labeled with the setOrderingFilter () function. Clustering analysis for dimensionality reduction was performed with reduceDimension (), max_components = 2, and reduction_method = "DDRTree," which was processed with the trajectory inference ("orderCells" function) using default parameters. Visualizations of gene expression were drawn as a special pseudotime trajectory function to track corresponding changes across the differentiation order, and this approach was also used for some marker genes relevant to developmental pseudotime.

Bulk RNA isolation, library construction, and transcriptome sequencing

The same treatments used in the scRNA-seq experiments were prepared with two portions, and undissociated root tips and dissociated protoplasts were separately subjected to RNA extraction (Liu et al., 2022a, 2022b, 2022c, 2022d). Total RNA was extracted from root samples or protoplasts with the RNAPrep Pure Plant Kit (Tiangen, Beijing, China) following the manufacturer's instructions. The quality and concentration of each RNA sample were determined with a NanoDrop 2000 spectrophotometer, and RNA samples with a 260/280 ratio in the range of 1.80–2.1 were used for further analysis. RNA quality was also determined by agarose gel electrophoresis and spectrophotometric analysis. The high-quality RNA was used for library construction and transcriptome sequencing, which were performed by Shanghai OE Biotech (Shanghai, China). Three biological replicates were performed for each group, for a total of 12 cDNA libraries. The Illumina HiSeq 2500 (Illumina, San Diego, CA) sequencing platform was used to sequence each cDNA library.

Identification and enrichment analyses of DEGs

The FindMarkers function (test.use = MAST) in Seurat (Butler et al., 2018) was used to identify DEGs among different treatments, and important genes with significant differential expression were identified using the threshold of $P < 0.05$ and $|\log 2 \text{ fold change}| > 2.0$. Analyses of GO and KEGG pathways were conducted on the DEGs to identify their potential functional enrichment (Kanehisa and Goto, 2000; Wilkerson and Hayes, 2010). The "clusterProfiler" R package was used to perform the enrichment analyses (Yu et al., 2012), and significantly enriched terms were identified using a threshold value of <0.05 for the false discovery rate.

In situ RNA hybridization

Five-day-old lateral roots of *G. arboreum* SXY1 grown under natural conditions were collected for paraffin sectioning and immediately fixed in FAA (10% formaldehyde, 5% acetic acid, and 47.5% ethanol) for 24 h. The fixed roots were then subjected to dehydration overnight, permeabilization for 7 h, wax dipping for 48 h, embedding for 24 h, slicing for 48 h, and mounting. Specific primers were designed for three representative marker genes, *Ga03G2153*, *Ga08G1867*, and *Ga05G0063*, (supplemental Table 3) to synthesize probes, and *in situ* hybridization and immunological detection were carried out as described previously (Liang et al., 2015).

VIGS of *GaGH3.6* and NaCl treatment

The tobacco rattle virus (TRV:00) plasmid was digested with restriction enzymes *Xba*I and *Kpn*I, which were combined with the target fragment to

generate TRV:*GaGH3.6* by specifically designed primers (supplemental Table 4). Subsequently, the correctly sequenced TRV:*GaGH3.6* plasmid was transformed into *Agrobacterium tumefaciens* LBA4404, which was mixed with auxiliary bacteria and infiltrated into 10-day-old cotyledons of *G. arboreum* SXY-1 seedlings (Peng et al., 2021). The cotton seedlings were grown in half-strength Hoagland nutrient solution with a 16-h light (25°C)/8-h dark (20°C) cycle and a relative humidity of 60%. Salt treatment (200 mM NaCl) was performed on seedlings with two true, fully expanded leaves, and real-time quantitative polymerase chain reaction (qPCR) experiments were used to determine silencing efficiency (Shiraku et al., 2021).

Total RNA was extracted from seedling leaves with the RNAPrep Pure Plant kit (Tiangen), and RNA quality was examined by gel electrophoresis and with a NanoDrop 2000 spectrophotometer (Thermo Scientific, Wilmington, DE). The high-quality mRNA was used for reverse transcription and cDNA synthesis with the TransScript All-in-One First-Strand cDNA Synthesis SuperMix for qPCR kit (Tiangen). Real-time qPCR was performed in a 20- μl system that included 2 μl cDNA, 6.6 μl deionized H₂O, 10 μl green qPCR SuperMix (Vazyme Biotech, Nanjing, China), 0.4 μl dye, and 0.5 μl forward and reverse primers. The housekeeping gene *Ubiquitin7* (*UB7*, GeneBank: DQ116441, supplemental Table 4) was used as the reference gene (Mo et al., 2019), and relative gene expression levels were calculated by the $2^{-\Delta\Delta\text{Ct}}$ method (Livak and Schmittgen, 2001).

Measurement of morphological, physiological, and biochemical features under salt stress

The WT, TRV:00, and TRV:*GaGH3.6* seedlings were cultured in nutrient medium with 200 mM NaCl for 4 weeks, and the corresponding morphological changes were assessed as described previously (Shiraku et al., 2021). All samples were collected at 48 h after 200 mM NaCl treatment, with three biological replicates. Leaf samples were used to monitor RLWC; their initial fresh weight (FW) was determined, and they were then soaked in ddH₂O for 24 h under a 16-h light/8-h dark photoperiod. The moisture on the leaf surface was then whisked away, and the saturated weight (SW) was recorded. Samples were placed into an oven at 80°C and dried for 24 h. Finally, their dry weight (DW) was recorded. RLWC was calculated as $(\text{FW} - \text{DW})/(\text{SW} - \text{DW}) \times 100\%$ (Shiraku et al., 2021). Diaminobenzidine (3,3'-N-diaminobenzidine [DAB]) staining of cotton leaves was used to detect the degree of oxidative damage. Samples were gently picked up with tweezers, placed into the DAB staining solution, and stained for more than 8 h in the dark. The DAB staining solution was poured off, 95% ethanol was added, and the samples were placed in a boiling water bath for 10 min until the background color of the plants was completely removed. The destaining solution was removed and replaced with absolute ethanol, and photographs of the leaf samples were taken for observation and comparison (Shiraku et al., 2021). Leaf ion leakage was measured as described previously (Mehari et al., 2021). Chlorophyll content was measured using 200-mg samples of cotton leaves, which were first snap-frozen in liquid nitrogen, then placed in 5 ml ethanol (99.9%) in a water bath at 80°C for 20 min. A suitable extinction coefficient was used, and chlorophyll content was calculated as $100 \times A654/(39.6 \times \text{FW})$ (Tetley and Thimann, 1974).

DATA AND CODE AVAILABILITY

The data discussed in this publication have been deposited in the Gene Expression Omnibus (GEO) of the NCBI (Edgar et al., 2002) and are accessible through GEO Series accession number GSE226218 (<https://www.ncbi.nlm.nih.gov/geo/query/acc.cgi?acc=GSE226218>).

SUPPLEMENTAL INFORMATION

Supplemental information is available at *Plant Communications Online*.

FUNDING

This work was supported by the National Natural Science Foundation of China (31471548, 32272179, and 31801404), the Central Plains Science and Technology Innovation Leader Project (214200510029), the Program for Innovative Research Team (in Science and Technology) in University of Henan Province (20IRTSTHN021), the Science and Technology Development Project of Anyang City (2022C01NY001 and 2022C01NY003), the Doctoral and Postdoctoral Research Fund of Anyang Institute of Technology (BSJ2019014 and BHJ2020002), the Key Scientific Research Project of Henan Higher Education Institutions of China (20A210006), and the Zhongyuan Scholars Workstation (224400510020).

AUTHOR CONTRIBUTIONS

F.L., S.J., and R.P. conceived the project. X.C., Z.Z., K.W., and B.Z. made suggestions for the project. Y.L., Q.L., N.H., T.W., S.C., Z.L., Z.Z., and Y.L. prepared the materials for protoplasts. P.L., Q.L., Y.W., and C.X. prepared the protoplasts. P.L., Q.L., Z.X., F.D., and X.Z. analyzed the data. P.L., Q.L., and Y.W. performed the RNA *in situ* hybridization experiments. P.L., Q.L., and J.H. performed the VIGS experiment. P.L., Q.L., Y.W., and C.X. wrote the paper. All authors discussed the results and commented on the manuscript. The authors read and approved the final manuscript.

ACKNOWLEDGMENTS

We sincerely thank Prof. Jiming Jiang (Department of Plant Biology, Michigan State University, East Lansing, MI, USA) for assistance with experimental design and article frame, and we also thank Dr. Xiaohua Yao and Hongyan Liu (OE Biotech Co., Ltd, Shanghai, China) for assistance with the bioinformatics analysis of scRNA-seq data. We thank LetPub (www letpub com), Dr. Baohong Zhang, and Dr. Shuangxia Jin for their linguistic assistance during the preparation of this manuscript. No conflict of interest is declared.

Received: October 2, 2022

Revised: March 2, 2023

Accepted: October 23, 2023

Published: October 29, 2023

REFERENCES

- Abbasi, A.R., Hajirezaei, M., Hofius, D., Sonnewald, U., and Voll, L.M.** (2007). Specific roles of alpha- and gamma-tocopherol in abiotic stress responses of transgenic tobacco. *Plant Physiol.* **143**:1720–1738. 1823.
- Aloni, R., Langhans, M., Aloni, E., Dreieicher, E., and Ullrich, C.I.** (2005). Root-synthesized cytokinin in *Arabidopsis* is distributed in the shoot by the transpiration stream. *J. Exp. Bot.* **56**:1535–1544.
- Apelt, F., Mavrothalassiti, E., Gupta, S., Machin, F., Olas, J.J., Annunziata, M.G., Schindeläsch, D., and Kragler, F.** (2022). Shoot and root single cell sequencing reveals tissue- and daytime-specific transcriptome profiles. *Plant Physiol.* **188**:861–878.
- Arif, M.R., Islam, M.T., and Robin, A.H.K.** (2019). Salinity stress alters root morphology and root hair traits in *Brassica napus*. *Plants* **8**:192.
- Atkinson, N.J., and Urwin, P.E.** (2012). The interaction of plant biotic and abiotic stresses: from genes to the field. *J. Exp. Bot.* **63**:3523–3543.
- Bai, Y., Liu, H., Lyu, H., Su, L., Xiong, J., and Cheng, Z.M.M.** (2022). Development of a single-cell atlas for woodland strawberry (*Fragaria vesca*) leaves during early *Botrytis cinerea* infection using single cell RNA-seq. *Hortic. Res.* **9**, uhab055.
- Becht, E., McInnes, L., Healy, J., Dutertre, C.A., Kwok, I.W.H., Ng, L.G., Ghinoux, F., and Newell, E.W.** (2018). Dimensionality reduction for visualizing single-cell data using UMAP. *Nat. Biotechnol.* **37**:38–44.
- Bennett, T., van den Toorn, A., Sanchez-Perez, G.F., Campilho, A., Willemsen, V., Snel, B., and Scheres, B.** (2010). SOMBRERO, Transcriptional landscape of cotton roots BEARSKIN1, and BEARSKIN2 regulate root cap maturation in *Arabidopsis*. *Plant Cell* **22**:640–654.
- Bernhardt, C., Zhao, M., Gonzalez, A., Lloyd, A., and Schiefelbein, J.** (2005). The bHLH genes GL3 and EGL3 participate in an intercellular regulatory circuit that controls cell patterning in the *Arabidopsis* root epidermis. *Development* **132**:291–298.
- Birnbaum, K., Shasha, D.E., Wang, J.Y., Jung, J.W., Lambert, G.M., Galbraith, D.W., and Benfey, P.N.** (2003). A gene expression map of the *Arabidopsis* root. *Science* **302**:1956–1960.
- Birnbaum, K.D.** (2018). Power in Numbers: Single-cell RNA-seq strategies to dissect complex tissues. *Annu. Rev. Genet.* **52**:203–221.
- Brady, S.M., Orlando, D.A., Lee, J.Y., Wang, J.Y., Koch, J., Dinneny, J.R., Mace, D., Ohler, U., and Benfey, P.N.** (2007). A high-resolution root spatiotemporal map reveals dominant expression patterns. *Science* **318**:801–806.
- Bray, E.A., Bailey-Serres, J., and Weretilnyk, E.** (2000). Biochemistry and Molecular Biology of Plants, Responses to Abiotic Stresses (American Society of Plant Biologists), pp. 1158–1249.
- Bu, Y., Takano, T., and Liu, S.** (2019). The role of ammonium transporter (AMT) against salt stress in plants. *Plant Signal. Behav.* **14**, 1625696.
- Butler, A., Hoffman, P., Smibert, P., Papalexi, E., and Satija, R.** (2018). Integrating single-cell transcriptomic data across different conditions, technologies, and species. *Nat. Biotechnol.* **36**:411–420.
- Cao, Y., Ma, J., Han, S., Hou, M., Wei, X., Zhang, X., Zhang, Z.J., Sun, S., Ku, L., Tang, J., et al.** (2023). Single-cell RNA sequencing profiles reveal cell type-specific transcriptional regulation networks conditioning fungal invasion in maize roots. *Plant Biotechnol. J.* **21**:1839–1859.
- Chambard, M., Ben Mlouka, M.A., Jing, L., Plasson, C., Cosette, P., Leprince, J., Follet-Gueye, M.L., Driouch, A., Nguema-Ona, E., and Boulogne, I.** (2022). Elicitation of roots and AC-DC with PEP-13 peptide shows differential defense responses in multi-omics. *Cells* **11**:2605.
- Chen, X., Xu, Z., Zhao, B., Yang, Y., Mi, J., Zhao, Z., and Liu, J.** (2022). Physiological and Proteomic Analysis Responsive Mechanisms for Salt Stress in Oat. *Front. Plant Sci.* **13**, 891674.
- Chen, Z., Nie, H., Grover, C.E., Wang, Y., Li, P., Wang, M., Pei, H., Zhao, Y., Li, S., Wendel, J.F., et al.** (2017). Entire nucleotide sequences of *Gossypium raimondii* and *G. arboreum* mitochondrial genomes revealed A-genome species as cytoplasmic donor of the allotetraploid species. *Plant Biol.* **19**:484–493.
- Cheong, M.S., Lee, D.Y., Seo, K.H., Choi, G.H., Song, Y.H., Park, K.H., and Kim, J.H.** (2019). Phenylephrine, a small molecule, inhibits pectin methylesterases. *Biochem. Biophys. Res. Commun.* **508**:320–325.
- Chun, H.J., Baek, D., Jin, B.J., Cho, H.M., Park, M.S., Lee, S.H., Lim, L.H., Cha, Y.J., Bae, D.W., Kim, S.T., et al.** (2021). Microtubule dynamics plays a vital role in plant adaptation and tolerance to salt stress. *Int. J. Mol. Sci.* **22**:5957.
- Cimini, S., Locato, V., Giacinti, V., Molinari, M., and De Gara, L.** (2022). A Multifactorial Regulation of Glutathione Metabolism behind Salt Tolerance in Rice. *Antioxidants* **11**:1114.
- Cocozza, C., Bartolini, P., Brunetti, C., Miozzi, L., Pignattelli, S., Podda, A., Scippa, G.S., Trupiano, D., Rotunno, S., Brilli, F., et al.** (2022). Modulation of class III peroxidase pathways and phenylpropanoids in *Arundo donax* under salt and phosphorus stress. *Plant Physiol. Biochem.* **183**:151–159.
- Damodaran, S., Westfall, C.S., Kisely, B.A., Jez, J.M., and Subramanian, S.** (2017). Nodule-enriched GRETCHEN HAGEN 3 enzymes have distinct substrate specificities and are important for proper soybean nodule development. *Int. J. Mol. Sci.* **18**:2547.

Transcriptional landscape of cotton roots

- Debbarma, J., Sarki, Y.N., Saikia, B., Boruah, H.P.D., Singha, D.L., and Chikkaputtaiah, C. (2019). Ethylene response factor (ERF) family proteins in abiotic stresses and CRISPR-Cas9 genome editing of ERFs for multiple abiotic stress tolerance in crop plants: A review. *Mol. Biotechnol.* **61**:153–172.
- Denyer, T., Ma, X., Klesen, S., Scacchi, E., Nieselt, K., and Timmermans, M.C.P. (2019). Spatiotemporal developmental trajectories in the *Arabidopsis* root revealed using high-throughput single-cell RNA sequencing. *Dev. Cell* **48**:840–852.e5.
- Du, X., Huang, G., He, S., Yang, Z., Sun, G., Ma, X., Li, N., Zhang, X., Sun, J., Liu, M., et al. (2018). Resequencing of 243 diploid cotton accessions based on an updated A genome identifies the genetic basis of key agronomic traits. *Nat. Genet.* **50**:796–802.
- Edgar, R., Domrachev, M., and Lash, A.E. (2002). Gene Expression Omnibus: NCBI gene expression and hybridization array data repository. *Nucleic Acids Res.* **30**:207–210.
- Efroni, I., Mello, A., Nawy, T., Ip, P.L., Rahni, R., DelRose, N., Powers, A., Satija, R., and Birnbaum, K.D. (2016). Root regeneration triggers an embryo-like sequence guided by hormonal interactions. *Cell* **165**:1721–1733.
- Espinosa, C., Liang, Y., and Stacey, G. (2017). Chitin receptor CERK1 links salt stress and chitin-triggered innate immunity in *Arabidopsis*. *Plant J.* **89**:984–995.
- Farhat, N., Hichri, S., Hildebrandt, T.M., Debez, A., and Braun, H.P. (2019). Composition and stability of the oxidative phosphorylation system in the halophile plant *Cakile maritima*. *Front. Plant Sci.* **10**:1010.
- Farmer, A., Thibivilliers, S., Ryu, K.H., Schiefelbein, J., and Libault, M. (2021). Single-nucleus RNA and ATAC sequencing reveals the impact of chromatin accessibility on gene expression in *Arabidopsis* roots at the single-cell level. *Mol. Plant* **14**:372–383.
- Foroozani, M., Holder, D.H., and Deal, R.B. (2022). Histone variants in the specialization of plant chromatin. *Annu. Rev. Plant Biol.* **73**:149–172.
- Franklin, R., Guo, Y., He, S., Chen, M., Ji, F., Zhou, X., Frankhouser, D., Do, B.T., Chiem, C., Jang, M., et al. (2022). Regulation of chromatin accessibility by the histone chaperone CAF-1 sustains lineage fidelity. *Nat. Commun.* **13**:2350.
- Fujita, K., and Inui, H. (2021). Review: Biological functions of major latex-like proteins in plants. *Plant Sci.* **306**, 110856.
- Gala, H.P., Lanctot, A., Jean-Baptiste, K., Guizou, S., Chu, J.C., Zemke, J.E., George, W., Queitsch, C., Cuperus, J.T., and Nemhauser, J.L. (2021). A single-cell view of the transcriptome during lateral root initiation in *Arabidopsis thaliana*. *Plant Cell* **33**:2197–2220.
- Gao, Y.F., Liu, J.K., Yang, F.M., Zhang, G.Y., Wang, D., Zhang, L., Ou, Y.B., and Yao, Y.A. (2020). The WRKY transcription factor WRKY8 promotes resistance to pathogen infection and mediates drought and salt stress tolerance in *Solanum lycopersicum*. *Physiol. Plantarum* **168**:98–117.
- García-Caparrós, P., Vogelsang, L., Persicke, M., Wirtz, M., Kumar, V., and Dietz, K.J. (2022). Differential sensitivity of metabolic pathways in sugar beet roots to combined salt, heat, and light stress. *Physiol. Plant* **174**:e13786.
- Gong, Z., Xiong, L., Shi, H., Yang, S., Herrera-Estrella, L.R., Xu, G., Chao, D.Y., Li, J., Wang, P.Y., Qin, F., et al. (2020). Plant abiotic stress response and nutrient use efficiency. *Sci. China Life Sci.* **63**:635–674.
- Graeff, M., Rana, S., Wendrich, J.R., Dorier, J., Eekhout, T., Aliaga Fandino, A.C., Guex, N., Bassel, G.W., De Rybel, B., and Hardtke, C.S. (2021). A single-cell morpho-transcriptomic map of brassinosteroid action in the *Arabidopsis* root. *Mol. Plant* **14**:1985–1999.

Plant Communications

- Guénin, S., Hardouin, J., Paynel, F., Müller, K., Mongelard, G., Driouch, A., Lerouge, P., Kermode, A.R., Lehner, A., Mollet, J.C., et al. (2017). AtPME3, a ubiquitous cell wall pectin methylesterase of *Arabidopsis thaliana*, alters the metabolism of cruciferin seed storage proteins during post-germinative growth of seedlings. *J. Exp. Bot.* **68**:1083–1095.
- Gutierrez, C. (2009). The *Arabidopsis* cell division cycle. *Arabidopsis Book* **7**, e0120.
- Haghverdi, L., Lun, A.T.L., Morgan, M.D., and Marioni, J.C. (2018). Batch effects in single-cell RNA-sequencing data are corrected by matching mutual nearest neighbors. *Nat. Biotechnol.* **36**:421–427.
- Hashemipetroudi, S.H., Ahmadian, G., Fatemi, F., Nematzadeh, G., Yamchi, A., and Kuhlmann, M. (2022). Ion content, antioxidant enzyme activity and transcriptional response under salt stress and recovery condition in the halophyte grass *Aeluropus littoralis*. *BMC Res. Notes* **15**:201.
- Hoang, X.L.T., Nhi, D.N.H., Thu, N.B.A., Thao, N.P., and Tran, L.S.P. (2017). Transcription factors and their roles in signal transduction in plants under abiotic stresses. *Curr. Genom.* **18**:483–497.
- Huan, L., Xie, X., Zheng, Z., Sun, F., Wu, S., Li, M., Gao, S., Gu, W., and Wang, G. (2014). Positive correlation between PSI response and oxidative pentose phosphate pathway activity during salt stress in an intertidal macroalga. *Plant Cell Physiol.* **55**:1395–1403.
- Huang, K.C., Lin, W.C., and Cheng, W.H. (2018). Salt hypersensitive mutant 9, a nucleolar APUM23 protein, is essential for salt sensitivity in association with the ABA signaling pathway in *Arabidopsis*. *BMC Plant Biol.* **18**:40.
- Ishimaru, Y., Hayashi, K., Suzuki, T., Fukaki, H., Prusinska, J., Meester, C., Quareshy, M., Egoshi, S., Matsuura, H., Takahashi, K., et al. (2018). Jasmonic acid inhibits auxin-induced lateral rooting independently of the CORONATINE INSENSITIVE1 Receptor. *Plant Physiol.* **177**:1704–1716.
- Jean-Baptiste, K., McFaline-Figueroa, J.L., Alexandre, C.M., Dorrit, M.W., Saunders, L., Bubb, K.L., Trapnell, C., Fields, S., Queitsch, C., and Cuperus, J.T. (2019). Dynamics of gene expression in single root cells of *Arabidopsis thaliana*. *Plant Cell* **31**:993–1011.
- Jia, C., Guo, B., Wang, B., Li, X., Yang, T., Li, N., Wang, J., and Yu, Q. (2022). Integrated metabolomic and transcriptomic analysis reveals the role of phenylpropanoid biosynthesis pathway in tomato roots during salt stress. *Front. Plant Sci.* **13**, 1023696.
- Jin, Y., Zhao, Y., Ai, S., Chen, X., Liu, X., Wang, H., Han, Y., Ma, F., and Li, C. (2022). Induction of polyploid *Malus prunifolia* and analysis of its salt tolerance. *Tree Physiol.* **42**:2100–2115.
- Kanehisa, M., and Goto, S. (2000). KEGG: kyoto encyclopedia of genes and genomes. *Nucleic Acids Res.* **28**:27–30.
- Kang, H., Wu, D., Fan, T., and Zhu, Y. (2020). Activities of chromatin remodeling factors and histone chaperones and their effects in root apical meristem development. *Int. J. Mol. Sci.* **21**:771.
- Kausar, R., and Komatsu, S. (2022). Proteomic approaches to uncover salt stress response mechanisms in crops. *Int. J. Mol. Sci.* **24**:518.
- Kim, J.Y., Symeonidi, E., Pang, T.Y., Denyer, T., Weidauer, D., Bezrutczyk, M., Miras, M., Zöllner, N., Hartwig, T., Wudick, M.M., Lercher, M., Chen, L.Q., Timmermans, M.C.P., and Frommer, W.B. (2021). Distinct identities of leaf phloem cells revealed by single cell transcriptomics. *Plant Cell* **33**:511–530.
- Kohli, P.S., Pazhamala, L.T., Mani, B., Thakur, J.K., and Giri, J. (2022). Root hair-specific transcriptome reveals response to low phosphorus in *Cicer arietinum*. *Front. Plant Sci.* **13**, 983969.
- Kolomeichuk, L.V., Efimova, M.V., Zlobin, I.E., Kreslavski, V.D., Murgan, O.K., Kovtun, I.S., Khripach, V.A., Kuznetsov, V.V., and Allakhverdiev, S.I. (2020). 24-Epibrassinolide alleviates the toxic

Plant Communications

- effects of NaCl on photosynthetic processes in potato plants. *Photosynth. Res.* **146**:151–163.
- Lberman, L.M., Sparks, E.E., Moreno-Risueno, M.A., Petricka, J.J., and Benfey, P.N.** (2015). MYB36 regulates the transition from proliferation to differentiation in the *Arabidopsis* root. *Proc. Natl. Acad. Sci. USA* **112**:12099–12104.
- Liu, M., Li, K., Sheng, S., Wang, M., Hua, P., Wang, Y., Chen, P., Wang, K., Zhao, M., Wang, Y., et al.** (2022a). Transcriptome analysis of MYB transcription factors family and PgMYB genes involved in salt stress resistance in Panax ginseng. *BMC Plant Biol.* **22**:479.
- Li, H., Dai, X., Huang, X., Xu, M., Wang, Q., Yan, X., Sederoff, R.R., and Li, Q.** (2021a). Single-cell RNA sequencing reveals a high-resolution cell atlas of xylem in *Populus*. *J. Integr. Plant Biol.* **63**:1906–1921.
- Li, M., Wang, M., Lin, Q., Wang, M., Niu, X., Cheng, J., Xu, M., Qin, Y., Liao, X., Xu, J., et al.** (2022). Symplastic communication in the root cap directs auxin distribution to modulate root development. *J. Integr. Plant Biol.* **64**:859–870.
- Li, X., Yu, B., Wu, Q., Min, Q., Zeng, R., Xie, Z., and Huang, J.** (2021b). OsMADS23 phosphorylated by SAPK9 confers drought and salt tolerance by regulating ABA biosynthesis in rice. *PLoS Genet.* **17**, e1009699.
- Liu, Z., Guo, C., Wu, R., Wang, J., Zhou, Y., Yu, X., Zhang, Y., Zhao, Z., Liu, H., Sun, S., et al.** (2022b). Identification of the Regulators of Epidermis Development under Drought- and Salt-Stressed Conditions by Single-Cell RNA-Seq. *Int. J. Mol. Sci.* **23**:2759.
- Liang, W., Cui, W., Ma, X., Wang, G., and Huang, Z.** (2014). Function of wheat Ta-UnP gene in enhancing salt tolerance in transgenic *Arabidopsis* and rice. *Biochem. Biophys. Res. Commun.* **450**:794–801.
- Liang, W., Ma, X., Wan, P., and Liu, L.** (2018). Plant salt-tolerance mechanism: A review. *Biochem. Biophys. Res. Commun.* **495**:286–291.
- Liang, Z., Brown, R.C., Fletcher, J.C., and Opsahl-Sorteberg, H.G.** (2015). Calpain-Mediated positional information directs cell wall orientation to sustain plant stem cell activity, growth and development. *Plant Cell Physiol.* **56**:1855–1866.
- Liu, H., Hu, D., Du, P., Wang, L., Liang, X., Li, H., Lu, Q., Li, S., Liu, H., Chen, X., et al.** (2021a). Single-cell RNA-seq describes the transcriptome landscape and identifies critical transcription factors in the leaf blade of the allotetraploid peanut (*Arachis hypogaea* L.). *Plant Biotechnol. J.* **19**:2261–2276.
- Liu, Q., Li, P., Cheng, S., Zhao, Z., Liu, Y., Wei, Y., Lu, Q., Han, J., Cai, X., Zhou, Z., et al.** (2022c). Protoplast dissociation and transcriptome analysis provides insights to salt stress response in cotton. *Int. J. Mol. Sci.* **23**:2845.
- Liu, Q., Liang, Z., Feng, D., Jiang, S., Wang, Y., Du, Z., Li, R., Hu, G., Zhang, P., Ma, Y., et al.** (2021b). Transcriptional landscape of rice roots at the single-cell resolution. *Mol. Plant* **14**:384–394.
- Liu, X., Tong, M., Zhang, A., Liu, M., Zhao, B., Liu, Z., Li, Z., Zhu, X., Guo, Y., and Li, R.** (2021c). COPII genes SEC31A/B are essential for gametogenesis and interchangeable in pollen development in *Arabidopsis*. *Plant J.* **105**:1600–1614.
- Liu, Z., Wang, J., Zhou, Y., Zhang, Y., Qin, A., Yu, X., Zhao, Z., Wu, R., Guo, C., Bawa, G., et al.** (2022d). Identification of novel regulators required for early development of vein pattern in the cotyledons by single-cell RNA-sequencing. *Plant J.* **110**:7–22.
- Liu, Z., Zhou, Y., Guo, J., Li, J., Tian, Z., Zhu, Z., Wang, J., Wu, R., Zhang, B., Hu, Y., et al.** (2020). Global dynamic molecular profiling of stomatal lineage cell development by single-cell rna sequencing. *Mol. Plant* **13**:1178–1193.
- Livak, K.J., and Schmittgen, T.D.** (2001). Analysis of relative gene expression data using real-time quantitative PCR and the 2(-Delta Delta C(T)) Method. *Methods* **25**:402–408.
- Transcriptional landscape of cotton roots**
- Lombardo, M.C., and Lamattina, L.** (2012). Nitric oxide is essential for vesicle formation and trafficking in *Arabidopsis* root hair growth. *J. Exp. Bot.* **63**:4875–4885.
- Long, L., Xu, F.C., Wang, C.H., Zhao, X.T., Yuan, M., Song, C.P., and Gao, W.** (2023). Single-cell transcriptome atlas identified novel regulators for pigment gland morphogenesis in cotton. *Plant Biotechnol. J.* **21**:1100–1102.
- Lu, H.P., Gao, Q., Han, J.P., Guo, X.H., Wang, Q., Altosaar, I., Barberon, M., Liu, J.X., Gatehouse, A.M.R., and Shu, Q.Y.** (2022). An ABA-serotonin module regulates root suberization and salinity tolerance. *New Phytol.* **236**:958–973.
- Lupo, Y., Schlisser, A., Dong, S., Rachmilevitch, S., Fait, A., and Lazarovitch, N.** (2022). Root system response to salt stress in grapevines (*Vitis* spp.): A link between root structure and salt exclusion. *Plant Sci.* **325**:111460.
- Macosko, E.Z., Basu, A., Satija, R., Nemesh, J., Shekhar, K., Goldman, M., Tirosh, I., Bialas, A.R., Kamitaki, N., Martersteck, E.M., et al.** (2015). Highly parallel genome-wide expression profiling of individual cells using nanoliter droplets. *Cell* **161**:1202–1214.
- Ma, J., Liu, Y., Zhou, W., Zhu, Y., Dong, A., and Shen, W.H.** (2018). Histone chaperones play crucial roles in maintenance of stem cell niche during plant root development. *Plant J.* **95**:86–100.
- Marand, A.P., Chen, Z., Gallavotti, A., and Schmitz, R.J.** (2021). A cis-regulatory atlas in maize at single-cell resolution. *Cell* **184**:3041–3055.e21.
- Mehari, T.G., Xu, Y., Magwanga, R.O., Umer, M.J., Shiraku, M.L., Hou, Y., Wang, Y., Wang, K., Cai, X., Zhou, Z., et al.** (2021). Identification and functional characterization of Gh_D01G0514 (*GhNAC072*) transcription factor in response to drought stress tolerance in cotton. *Plant Physiol. Biochem.* **166**:361–375.
- Melniky, C.W., Molnar, A., Bassett, A., and Baulcombe, D.C.** (2011). Mobile 24 nt small RNAs direct transcriptional gene silencing in the root meristems of *Arabidopsis thaliana*. *Curr. Biol.* **21**:1678–1683.
- Meyer, E.H., Tomaz, T., Carroll, A.J., Estavillo, G., Delannoy, E., Tanz, S.K., Small, I.D., Pogson, B.J., and Millar, A.H.** (2009). Remodeled respiration in ndufs4 with low phosphorylation efficiency suppresses *Arabidopsis* germination and growth and alters control of metabolism at night. *Plant Physiol.* **151**:603–619.
- Michelet, J.F., Olive, C., Rieux, E., Fagot, D., Simonetti, L., Galey, J.B., Dalko-Csiba, M., Bernard, B.A., and Pereira, R.** (2012). The anti-ageing potential of a new jasmonic acid derivative (LR2412): in vitro evaluation using reconstructed epidermis Episkin™. *Exp. Dermatol.* **21**:398–400.
- Mo, H., Wang, L., Ma, S., Yu, D., Lu, L., Yang, Z., Yang, Z., and Li, F.** (2019). Transcriptome profiling of *Gossypium arboreum* during fiber initiation and the genome-wide identification of trihelix transcription factors. *Gene* **709**:36–47.
- Mochizuki, S., Harada, A., Inada, S., Sugimoto-Shirasu, K., Stacey, N., Wada, T., Ishiguro, S., Okada, K., and Sakai, T.** (2005). The *Arabidopsis* WAVY GROWTH 2 protein modulates root bending in response to environmental stimuli. *Plant Cell* **17**:537–547.
- Morton, M.J.L., Awlia, M., Al-Tamimi, N., Saade, S., Pailles, Y., Negrão, S., and Tester, M.** (2019). Salt stress under the scalpel - dissecting the genetics of salt tolerance. *Plant J.* **97**:148–163.
- Nanda, A.K., El Habti, A., Hocart, C.H., and Masle, J.** (2019). ERECTA receptor-kinases play a key role in the appropriate timing of seed germination under changing salinity. *J. Exp. Bot.* **70**:6417–6435.
- Nelms, B., and Walbot, V.** (2019). Defining the developmental program leading to meiosis in maize. *Science* **364**:52–56.
- Omary, M., Gil-Yarom, N., Yahav, C., Steiner, E., Hendelman, A., and Efroni, I.** (2022). A conserved superlocus regulates above- and belowground root initiation. *Science* **375**, eabf4368.

Transcriptional landscape of cotton roots

- Pan, Y., Hu, X., Li, C., Xu, X., Su, C., Li, J., Song, H., Zhang, X., and Pan, Y. (2017). SlbZIP38, a tomato bZIP family gene downregulated by abscisic acid, is a negative regulator of drought and salt stress tolerance. *Genes* **8**:402.
- Peng, Z., Jiang, X., Wang, Z., Wang, X., Li, H., He, S., Pan, Z., Qayyum, A., Rehman, A., and Du, X. (2021). Identification of Raf-Like kinases B subfamily genes in *Gossypium* species revealed GhRAF42 enhanced salt tolerance in cotton. *Int. J. Mol. Sci.* **22**, 12649.
- Qin, Y., Sun, M., Li, W., Xu, M., Shao, L., Liu, Y., Zhao, G., Liu, Z., Xu, Z., You, J., et al. (2022). Single-cell RNA-seq reveals fate determination control of an individual fibre cell initiation in cotton (*Gossypium hirsutum*). *Plant Biotechnol. J.* **20**:2372–2388.
- Que, F., Wang, G.L., Xu, Z.S., Wang, F., and Xiong, A.S. (2017). Transcriptional regulation of brassinosteroid accumulation during carrot development and the potential role of brassinosteroids in petiole elongation. *Front. Plant Sci.* **8**:1356.
- Rajendran, S., and Kim, C.M. (2022). OsCSLD1 mediates NH₄⁺-dependent root hair growth suppression and AMT1;2 expression in rice (*Oryza sativa* L.). *Plants* **11**:3580.
- Reddy, G.V., Heisler, M.G., Ehrhardt, D.W., and Meyerowitz, E.M. (2004). Real-time lineage analysis reveals oriented cell divisions associated with morphogenesis at the shoot apex of *Arabidopsis thaliana*. *Development* **131**:4225–4237.
- Rehman, H.M., Chen, S., Zhang, S., Khalid, M., Uzair, M., Wilmarth, P.A., Ahmad, S., and Lam, H.M. (2022). Membrane proteomic profiling of soybean leaf and root tissues uncovers salt-stress-responsive membrane proteins. *Int. J. Mol. Sci.* **23**, 13270.
- Ryu, K.H., Huang, L., Kang, H.M., and Schiebelbein, J. (2019). Single-Cell RNA sequencing resolves molecular relationships among individual plant cells. *Plant Physiol.* **179**:1444–1456.
- Satterlee, J.W., Strable, J., and Scanlon, M.J. (2020). Plant stem-cell organization and differentiation at single-cell resolution. *Proc. Natl. Acad. Sci. USA* **117**:33689–33699.
- Serrano-Ron, L., Perez-Garcia, P., Sanchez-Corriñero, A., Gude, I., Cabrera, J., Ip, P.L., Birnbaum, K.D., and Moreno-Risueno, M.A. (2021). Reconstruction of lateral root formation through single-cell RNA sequencing reveals order of tissue initiation. *Mol. Plant* **14**:1362–1378.
- Seyfferth, C., Renema, J., Wendrich, J.R., Eekhout, T., Seurinck, R., Vandamme, N., Blob, B., Saeyns, Y., Helariutta, Y., Birnbaum, K.D., et al. (2021). Advances and opportunities in single-cell transcriptomics for plant research. *Annu. Rev. Plant Biol.* **72**:847–866.
- Shahan, R., Hsu, C.W., Nolan, T.M., Cole, B.J., Taylor, I.W., Greenstreet, L., Zhang, S., Afanassiev, A., Vlot, A.H.C., Schiebinger, G., et al. (2022). A single-cell *Arabidopsis* root atlas reveals developmental trajectories in wild-type and cell identity mutants. *Dev. Cell* **57**:543–560.e9.
- Sharma, K., Sharma, S., Vaishnav, A., Jain, R., Singh, D., Singh, H.B., Goel, A., and Singh, S. (2022). Salt-tolerant PGPR strain *Priestia endophytica* SK1 promotes fenugreek growth under salt stress by inducing nitrogen assimilation and secondary metabolites. *J. Appl. Microbiol.* **133**:2802–2813.
- Sheikhalipour, M., Esmaelpour, B., Gohari, G., Haghghi, M., Jafari, H., Farhadi, H., Kulak, M., and Kalisz, A. (2021). Salt Stress Mitigation via the Foliar Application of Chitosan-Functionalized Selenium and Anatase Titanium Dioxide Nanoparticles in Stevia (*Stevia rebaudiana* Bertoni). *Molecules* **26**:4090.
- Shiraku, M.L., Magwanga, R.O., Cai, X., Kirungu, J.N., Xu, Y., Mehari, T.G., Hou, Y., Wang, Y., Agong, S.G., Peng, R., et al. (2021). Functional Characterization of GhACX3 gene reveals its significant role in enhancing drought and salt stress tolerance in cotton. *Front. Plant Sci.* **12**, 658755.
- Shulse, C.N., Cole, B.J., Ciobanu, D., Lin, J., Yoshinaga, Y., Gouran, M., Turco, G.M., Zhu, Y., O'Malley, R.C., Brady, S.M., et al. (2019). High-throughput single-cell transcriptome profiling of plant cell types. *Cell Rep.* **27**:2241–2247.e4.
- Singh, D., Debnath, P., Sane, A.P., and Sane, V.A. (2023). Tomato (*Solanum lycopersicum*) WRKY23 enhances salt and osmotic stress tolerance by modulating the ethylene and auxin pathways in transgenic *Arabidopsis*. *Plant Physiol. Biochem.* **195**:330–340.
- Song, J.H., Montes-Luz, B., Tadra-Sfeir, M.Z., Cui, Y., Su, L., Xu, D., and Stacey, G. (2022). High-resolution translatome analysis reveals cortical cell programs during early soybean nodulation. *Front. Plant Sci.* **13**, 820348.
- Sun, X., Wang, Y., and Sui, N. (2018). Transcriptional regulation of bHLH during plant response to stress. *Biochem. Biophys. Res. Commun.* **503**:397–401.
- Sun, Y., Han, Y., Sheng, K., Yang, P., Cao, Y., Li, H., Zhu, Q.H., Chen, J., Zhu, S., and Zhao, T. (2023). Single-cell transcriptomic analysis reveals the developmental trajectory and transcriptional regulatory networks of pigment glands in *Gossypium bickii*. *Mol. Plant* **16**:694–708.
- Takatsuka, H., and Umeda, M. (2014). Hormonal control of cell division and elongation along differentiation trajectories in roots. *J. Exp. Bot.* **65**:2633–2643.
- Tang, F., Barbacioru, C., Wang, Y., Nordman, E., Lee, C., Xu, N., Wang, X., Bodeau, J., Tuch, B.B., Siddiqui, A., et al. (2009). mRNA-Seq whole-transcriptome analysis of a single cell. *Nat. Methods* **6**:377–382.
- Tetley, R.M., and Thimann, K.V. (1974). The Metabolism of Oat Leaves during Senescence: I. Respiration, Carbohydrate Metabolism, and the Action of Cytokinins. *Plant Physiol.* **54**:294–303.
- Tian, C., Du, Q., Xu, M., Du, F., and Jiao, Y. (2020). Single-nucleus RNA-seq resolves spatiotemporal developmental trajectories in the tomato shoot apex. Preprint at bioRxiv.
- Trapnell, C., Cacchiarelli, D., Grimsby, J., Pokharel, P., Li, S., Morse, M., Lennon, N.J., Livak, K.J., Mikkelsen, T.S., and Rinn, J.L. (2014). The dynamics and regulators of cell fate decisions are revealed by pseudotemporal ordering of single cells. *Nat. Biotechnol.* **32**:381–386.
- Turco, G.M., Rodriguez-Medina, J., Siebert, S., Han, D., Valderrama-Gómez, M.Á., Vahldick, H., Shulse, C.N., Cole, B.J., Juliano, C.E., Dickel, D.E., et al. (2019). Molecular mechanisms driving switch behavior in xylem cell differentiation. *Cell Rep.* **28**:342–351.e4.
- Vaghela, B., Vashi, R., Rajput, K., and Joshi, R. (2022). Plant chitinases and their role in plant defense: A comprehensive review. *Enzyme Microb. Technol.* **159**:110055.
- van Engelen, F.A., Hartog, M.V., Thomas, T.L., Taylor, B., Sturm, A., van Kammen, A., and de Vries, S.C. (1993). The carrot secreted glycoprotein gene EP1 is expressed in the epidermis and has sequence homology to *Brassica* S-locus glycoproteins. *Plant J.* **4**:855–862.
- van Hengel, A.J., Barber, C., and Roberts, K. (2004). The expression patterns of arabinogalactan-protein AtAGP30 and GLABRA2 reveal a role for abscisic acid in the early stages of root epidermal patterning. *Plant J.* **39**:70–83.
- Velandia, K., Reid, J.B., and Foo, E. (2022). Right time, right place: The dynamic role of hormones in rhizobial infection and nodulation of legumes. *Plant Commun.* **3**:100327.

Plant Communications

Plant Communications

- Verma, S., Negi, N.P., Pareek, S., Mudgal, G., and Kumar, D.** (2022). Auxin response factors in plant adaptation to drought and salinity stress. *Physiol. Plantarum* **174**, e13714.
- Wan, J., Torres, M., Ganapathy, A., Thelen, J., DaGue, B.B., Mooney, B., Xu, D., and Stacey, G.** (2005). Proteomic analysis of soybean root hairs after infection by *Bradyrhizobium japonicum*. *Mol. Plant Microbe Interact.* **18**:458–467.
- Wang, C., Chen, L., Cai, Z., Chen, C., Liu, Z., Liu, S., Zou, L., Tan, M., Chen, J., Liu, X., et al.** (2021a). Metabolite profiling and transcriptome analysis explains difference in accumulation of bioactive constituents in Licorice (*Glycyrrhiza uralensis*) under salt stress. *Front. Plant Sci.* **12**, 727882.
- Wang, L., Ning, Y., Sun, J., Wilkins, K.A., Matthus, E., McNelly, R.E., Dark, A., Rubio, L., Moeder, W., Yoshioka, K., et al.** (2022). *Arabidopsis thaliana* CYCLIC NUCLEOTIDE-GATED CHANNEL2 mediates extracellular ATP signal transduction in root epidermis. *New Phytol.* **234**:412–421.
- Wang, S., Shi, M., Zhang, Y., Xie, X., Sun, P., Fang, C., and Zhao, J.** (2021b). FvMYB24, a strawberry R2R3-MYB transcription factor, improved salt stress tolerance in transgenic *Arabidopsis*. *Biochem. Biophys. Res. Commun.* **569**:93–99.
- Wang, W., Ryu, K.H., Bruex, A., Barron, C., and Schiefelbein, J.** (2020a). Molecular basis for a cell fate switch in response to impaired ribosome biogenesis in the *Arabidopsis* root epidermis. *Plant Cell* **32**:2402–2423.
- Wang, T.T., Yu, T.F., Fu, J.D., Su, H.G., Chen, J., Zhou, Y.B., Chen, M., Guo, J., Ma, Y.Z., Wei, W.L., et al.** (2020b). Genome-Wide Analysis of the GRAS gene family and functional identification of GmGRAS37 in drought and salt tolerance. *Front. Plant Sci.* **11**, 604690.
- Wang, Y., Huan, Q., Li, K., and Qian, W.** (2021c). Single-cell transcriptome atlas of the leaf and root of rice seedlings. *J Genet Genomics* **48**:881–898.
- Wang, P., Wang, C.M., Gao, L., Cui, Y.N., Yang, H.L., de Silva, N.D.G., Ma, Q., Bao, A.K., Flowers, T.J., Rowland, O., et al.** (2020c). Aliphatic suberin confers salt tolerance to *Arabidopsis* by limiting Na⁺ influx, K⁺ efflux and water backflow. *Plant Soil* **448**:603–620.
- Wei, J., Liang, J., Liu, D., Liu, Y., Liu, G., and Wei, S.** (2022). Melatonin-induced physiology and transcriptome changes in banana seedlings under salt stress conditions. *Front. Plant Sci.* **13**:938262.
- Wen, L., and Tang, F.** (2022). Recent advances in single-cell sequencing technologies. *Precis. Clin. Med.* **5**:pbac002.
- Wendel, J.F., Flagel, L.E., and Adams, K.L.** (2012). Jeans, Genes, and Genomes: Cotton as a Model for Studying Polyploidy. In *Polyploidy and Genome Evolution*, P. Soltis and D. Soltis, eds. (Springer), pp. 181–207.
- Wendrich, J.R., Yang, B., Vandamme, N., Verstaen, K., Smet, W., Van de Velde, C., Minne, M., Wybouw, B., Mor, E., Arents, H.E., et al.** (2020). Vascular transcription factors guide plant epidermal responses to limiting phosphate conditions. *Science* **370**, eaay4970.
- White, P.J.** (2001). The pathways of calcium movement to the xylem. *J. Exp. Bot.* **52**:891–899.
- Wilkerson, M.D., and Hayes, D.N.** (2010). ConsensusClusterPlus: a class discovery tool with confidence assessments and item tracking. *Bioinformatics* **26**:1572–1573.
- Wu, H., Ye, H., Yao, R., Zhang, T., and Xiong, L.** (2015). OsJAZ9 acts as a transcriptional regulator in jasmonate signaling and modulates salt stress tolerance in rice. *Plant Sci.* **232**:1–12.
- Xiao, R., Zhang, C., Guo, X., Li, H., and Lu, H.** (2021). MYB transcription factors and its regulation in secondary cell wall formation and lignin biosynthesis during xylem development. *Int. J. Mol. Sci.* **22**:3560.
- Transcriptional landscape of cotton roots**
- Xie, J., Li, M., Zeng, J., Li, X., and Zhang, D.** (2022). Single-cell RNA sequencing profiles of stem-differentiating xylem in poplar. *Plant Biotechnol. J.* **20**:417–419.
- Xu, X., Crow, M., Rice, B.R., Li, F., Harris, B., Liu, L., Demesa-Arevalo, E., Lu, Z., Wang, L., Fox, N., et al.** (2021). Single-cell RNA sequencing of developing maize ears facilitates functional analysis and trait candidate gene discovery. *Dev. Cell* **56**:557–568.e6.
- Xu, Z., Wang, Q., Zhu, X., Wang, G., Qin, Y., Ding, F., Tu, L., Daniell, H., Zhang, X., and Jin, S.** (2022). Plant Single Cell Transcriptome Hub (Pscth): an integrated online tool to explore the plant single-cell transcriptome landscape. *Plant Biotechnol. J.* **20**:10–12.
- Yang, S., Liu, M., Chu, N., Chen, G., Wang, P., Mo, J., Guo, H., Xu, J., and Zhou, H.** (2022). Combined transcriptome and metabolome reveal glutathione metabolism plays a critical role in resistance to salinity in rice landraces HD961. *Front. Plant Sci.* **13**:952595.
- Ye, L., Cao, L., Zhao, X., Guo, X., Ye, K., Jiao, S., Wang, Y., He, X., Dong, C., Hu, B., et al.** (2022). Investigation of the JASMONATE ZIM-DOMAIN gene family reveals the canonical ja-signaling pathway in pineapple. *Biology* **11**:445.
- Yu, G., Wang, L.G., Han, Y., and He, Q.Y.** (2012). clusterProfiler: an R package for comparing biological themes among gene clusters. *OMICS* **16**:284–287.
- Yu, Z., Duan, X., Luo, L., Dai, S., Ding, Z., and Xia, G.** (2020). How Plant Hormones Mediate Salt Stress Responses. *Trends Plant Sci.* **25**:1117–1130.
- Zhai, N., and Xu, L.** (2021). Pluripotency acquisition in the middle cell layer of callus is required for organ regeneration. *Nat. Plants* **7**:1453–1460.
- Zhang, H., Guo, L., Li, Y., Zhao, D., Liu, L., Chang, W., Zhang, K., Zheng, Y., Hou, J., Fu, C., et al.** (2022a). TOP1 α fine-tunes TOR-PLT2 to maintain root tip homeostasis in response to sugars. *Nat. Plants* **8**:792–801.
- Zhang, H., Zhao, Y., and Zhu, J.K.** (2020). Thriving under Stress: How Plants Balance Growth and the Stress Response. *Dev. Cell* **7**:529–543.
- Zhang, L., Wang, L., Chen, X., Zhao, L., Liu, X., Wang, Y., Wu, G., Xia, C., Zhang, L., and Kong, X.** (2022b). The protein phosphatase 2C clade A TaPP2CA interact with calcium-dependent protein kinases, TaCDPK5/TaCDPK9-1, that phosphorylate TabZIP60 transcription factor from wheat (*Triticum aestivum* L.). *Plant Sci.* **321**, 111304.
- Zhang, Q., Deng, A., Xiang, M., Lan, Q., Li, X., Yuan, S., Gou, X., Hao, S., Du, J., and Xiao, C.** (2022c). The Root hair development of pectin polygalacturonase PGX2 activation tagging line in response to phosphate deficiency. *Front. Plant Sci.* **13**, 862171.
- Zhang, T.Q., Chen, Y., Liu, Y., Lin, W.H., and Wang, J.W.** (2021a). Single-cell transcriptome atlas and chromatin accessibility landscape reveal differentiation trajectories in the rice root. *Nat. Commun.* **12**:2053.
- Zhang, T.Q., Chen, Y., and Wang, J.W.** (2021b). A single-cell analysis of the *Arabidopsis* vegetative shoot apex. *Dev. Cell* **56**:1056–1074.e8.
- Zhang, T.Q., Xu, Z.G., Shang, G.D., and Wang, J.W.** (2019a). A Single-Cell RNA Sequencing Profiles the Developmental Landscape of *Arabidopsis* Root. *Mol. Plant* **12**:648–660.
- Zhang, Y., Li, D., Zhou, R., Wang, X., Dossa, K., Wang, L., Zhang, Y., Yu, J., Gong, H., Zhang, X., et al.** (2019b). Transcriptome and metabolome analyses of two contrasting sesame genotypes reveal the crucial biological pathways involved in rapid adaptive response to salt stress. *BMC Plant Biol.* **19**:66.
- Zhao, G., Song, Y., Wang, Q., Yao, D., Li, D., Qin, W., Ge, X., Yang, Z., Xu, W., Su, Z., et al.** (2020). *Gossypium hirsutum* salt tolerance is enhanced by overexpression of *G. arboreum* JAZ1. *Front. Bioeng. Biotechnol.* **8**:157.

Transcriptional landscape of cotton roots

Zhao, H., Li, Z., Wang, Y., Wang, J., Xiao, M., Liu, H., Quan, R., Zhang, H., Huang, R., Zhu, L., et al. (2022). Cellulose synthase-like protein OsCSLD4 plays an important role in the response of rice to salt stress by mediating abscisic acid biosynthesis to regulate osmotic stress tolerance. *Plant Biotechnol. J.* **20**:468–484.

Zheng, G.X.Y., Terry, J.M., Belgrader, P., Ryvkin, P., Bent, Z.W., Wilson, R., Zraldo, S.B., Wheeler, T.D., McDermott, G.P., Zhu, J.,

Plant Communications

et al. (2017). Massively parallel digital transcriptional profiling of single cells. *Nat. Commun.* **8**, 14049.

Zhou, S., Chen, Q., Sun, Y., and Li, Y. (2017). Histone H2B monoubiquitination regulates salt stress-induced microtubule depolymerization in *Arabidopsis*. *Plant Cell Environ.* **40**:1512–1530.

Zhu, J.K. (2016). Abiotic Stress Signaling and Responses in Plants. *Cell* **167**:313–324.